

THESIS FOR THE DEGREE OF DOCTOR OF PHILOSOPHY

# **Stability of Bulk-Heterojunction Blends for Solar Cell Applications**

CAMILLA LINDQVIST



Applied Chemistry/Polymer Technology  
Department of Chemical and Biological Engineering  
CHALMERS UNIVERSITY OF TECHNOLOGY  
Göteborg, Sweden 2014

# **STABILITY OF BULK-HETEROJUNCTION BLENDS FOR SOLAR CELL APPLICATIONS**

CAMILLA LINDQVIST

© CAMILLA LINDQVIST, 2014  
ISBN 978-91-7385-982-0

Doktorsavhandlingar vid Chalmers tekniska högskola  
Ny serie nr 3663  
ISSN 0346-718X

Applied Chemistry/Polymer Technology  
Department of Chemical and Biological Engineering  
Chalmers University of Technology  
SE-412 96 Gothenburg  
Sweden  
Telephone + 46 (0) 31-772 10 00

Cover: Drop-casted film of 1:1 TQ1:PC<sub>61</sub>BM annealed at 150 °C for 10 min.

Chalmers Reproservice  
Gothenburg, Sweden 2014

## **Stability of Bulk-Heterojunction Blends for Solar Cell Applications**

CAMILLA LINDQVIST

*Department of Chemical and Biological Engineering*

Chalmers University of Technology

Gothenburg, Sweden

### **ABSTRACT**

---

Polymer solar cells are a promising alternative to more traditional silicon solar cells. This is mainly due to the good solubility of organic semiconductors, which makes it possible to produce large-scale and mechanically flexible devices with roll-to-roll processes. To be able to fully utilise this promising technique the stability of the materials, used in these devices, must be guaranteed.

The focus of this thesis is the stability of the active layers of polymer solar cells. Both, bleaching due to photo-oxidative degradation and thermal stability of the nanostructure have been studied. The presented work is mostly based on blends of a thiophene-quinoxaline based polymer (TQ1) and fullerene derivatives (PCBM).

The first part of the thesis deals with the photo-oxidative stability of TQ1 and a pyrido pyrazine based polymer (TQN). To make those polymers more black they were co-polymerised with thiophene-hexylthiophene. The stability of TQN is shown to be un-effected by this incorporation whereas the stability of TQ1 decreased. Moreover, the degradation rate of TQ1 seems to be independent of both molecular weight and film thickness.

The stability of the nanostructure has been studied with various microscopy and spectroscopy methods. Below the glass transition temperature of the TQ1:PC<sub>61</sub>BM blend only local rearrangement of polymer chains is possible. This mild annealing is found to increase the device efficiency. In contrast, annealing at higher temperatures above the glass transition temperature led to a coarser nanostructure and formation of PCBM crystals, which was detrimental for the performance of

corresponding solar cells. Finally, this thesis demonstrates that the thermal stability of these blends can be significantly improved by inclusion of neat C<sub>60</sub>-fullerene as well as the use of a mixture of two fullerene derivatives as the acceptor material.

**Keywords:** *Polymer solar cells, bulk-heterojunction, stability, nanostructure, PCBM crystallisation*

## LIST OF PUBLICATIONS

---

This thesis is based on the following scientific papers, referred to by their Roman numerals in the text. The papers are appended at the end of the thesis.

Paper I. **Stability study of quinoxaline and pyrido pyrazine based co-polymers for solar cell applications**

Patrik Henriksson, Camilla Lindqvist, Bedasa Abdisa Gonfa, Ergang Wang, Zandra George, Renee Kroon, Christian Müller, Teketel Yohannes, Olle Inganäs, Mats R. Andersson

*Manuscript*

Paper II. **Facile Monitoring of Fullerene Crystallization in Polymer Solar Cell Blends by UV-Vis Spectroscopy**

Camilla Lindqvist, Ergang Wang, Mats R. Andersson, Christian Müller

*Macromolecular Chemistry and Physics 2014, DOI: 10.1002/macp.201300717*

Paper III. **Sub-glass transition annealing enhances polymer solar cell performance**

Jonas Bergqvist, Camilla Lindqvist, Olof Bäcke, Zaifei Ma, Zheng Tang, Wolfgang Tress, Stefan Gustafsson, Ergang Wang, Eva Olsson, Mats R. Andersson, Olle Inganäs, Christian Müller

*Journal of Materials Chemistry A 2014, DOI: 10.1039/c3ta14165a*

Paper IV. **Nucleation-limited fullerene crystallisation in a polymer–fullerene bulk-heterojunction blend**

Camilla Lindqvist, Anke Sanz-Velasco, Ergang Wang, Olof Bäcke, Stefan Gustafsson, Eva Olsson, Mats R. Andersson, Christian Müller

*Journal of Materials Chemistry A 2013, 1, 7174-7180*

**Paper V. Fullerene Nucleating Agents: A Route towards Thermally Stable Photovoltaic Blends**

Camilla Lindqvist, Jonas Bergqvist, Ching-Chiao Feng, Stefan Gustafsson, Olof Bäcke, Neil D. Treat, Céline Bounioux, Patrik Henriksson, Renee Kroon, Ergang Wang, Anke Sanz-Velasco, Per Magnus Kristiansen, Natalie Stingelin, Eva Olsson, Olle Inganäs, Mats R. Andersson, Christian Müller

*Accepted in Advanced Energy Materials, 2014*

**Paper VI. Fullerene mixtures enhance the thermal stability of a non-crystalline polymer solar cell blend**

Camilla Lindqvist, Jonas Bergqvist, Olof Bäcke, Stefan Gustafsson, Ergang Wang, Eva Olsson, Olle Inganäs, Mats R. Andersson, Christian Müller

*Manuscript*

# CONTRIBUTION REPORT

---

- Paper I.** Performed and analysed the stability measurements. Shared main authorship with Patrik Henriksson.
- Paper II.** Collected and analysed the data. Wrote the paper.
- Paper III.** Collected and analysed the data together with Jonas Bergqvist (LiU). TEM was carried out by Olof Bäcké and Stefan Gustafsson (Chalmers). Wrote the manuscript together with co-authors.
- Paper IV.** Collected and analysed the data. TEM was carried out by Olof Bäcké and Stefan Gustafsson (Chalmers), SEM was carried out in collaboration with Anke Sanz-Velasco (Chalmers). Wrote the manuscript together with co-authors.
- Paper V.** Collected and analysed the data. TEM was carried out by Olof Bäcké and Stefan Gustafsson (Chalmers), SEM was carried out in collaboration with Anke Sanz-Velasco (Chalmers). Wrote the manuscript together with co-authors.
- Paper VI.** Collected and analysed the data. TEM was carried out by Olof Bäcké and Stefan Gustafsson (Chalmers). Solar cell characterisation was performed by Jonas Bergqvist (LiU). Wrote the manuscript together with co-authors.

## **PUBLICATIONS NOT INCLUDED IN THE THESIS**

---

Paper VII. **Effect of electron-withdrawing side chain modifications on the optical properties of thiophene-quinoxaline acceptor based polymers**

Renee Kroon, Angelica Lundin, Camilla Lindqvist, Patrik Henriksson, Timothy T.

Steckler, Mats R. Andersson

*Polymer*, 2013, **54**, 1285-1288



# TABLE OF CONTENTS

---

---

<b>Chapter 1 - INTRODUCTION .....</b>	<b>1</b>
<b>Chapter 2 - POLYMER SOLAR CELLS .....</b>	<b>5</b>
2.1 Background .....	5
2.2 Conjugated polymers.....	5
2.3 Fullerene derivatives .....	9
2.4 Bulk-heterojunctions .....	11
2.5 Characterisation of the nanostructure .....	12
2.5.1. <i>Optical microscopy</i> .....	12
2.5.3. <i>Scanning electron microscopy</i> .....	13
2.5.5. <i>Spectroscopic methods</i> .....	14
2.6 Device architecture.....	15
2.5.1. <i>Conventional device architecture</i> .....	15
2.5.2. <i>Inverted device architecture</i> .....	16
2.7 Working principle of polymer solar cells.....	17
2.8 IV-characteristics .....	19
2.8 Lifetime and stability of devices .....	20
2.9 Processing techniques for large scale devices .....	21
<b>Chapter 3 - PHOTO-INDUCED DEGRADATION.....</b>	<b>23</b>

3.1 Degradation of the donor polymer .....	23
3.2 Degradation of PCBM.....	25
3.3 Stability enhancement .....	25
3.3.1. PCBM .....	25
3.3.2. <i>Polymers with thermo-cleavable side chains</i> .....	25
3.3.3. <i>UV-stabilisers</i> .....	26
3.3.4. <i>Encapsulation and protecting layers</i> .....	26
3.4 Photo-oxidative stability of TQ1 .....	26
3.4.1 <i>Incorporation of thiophene-hexylthiophene units</i> .....	27
3.4.2. <i>Influence of molecular weight</i> .....	29
3.4.3. <i>Influence of film thickness</i> .....	30
<b>Chapter 4 - THERMAL STABILITY OF THE BULK-HETEROJUNCTION BLEND.....</b>	<b>31</b>
4.1 Background .....	31
4.1.1 <i>Thermal transitions</i> .....	32
4.1.2. <i>Phase separation and fullerene crystallisation in BHJ blends</i> .....	33
4.1.3 <i>Determination of thermal transitions</i> .....	33
4.1.4 <i>Thermal transitions of materials encountered in this thesis</i> .....	34
4.2 Using the onset of PC <sub>61</sub> BM crystallisation to determine the upper limit of the glass transition temperature.....	35

4.3 Annealing of TQ1:PC <sub>61</sub> BM films below the glass transition temperature	37
4.4 Annealing of TQ1:PC <sub>61</sub> BM films above glass transition temperature	39
4.5 Improving the thermal stability of TQ1:PC <sub>61</sub> BM blends	42
4.5.1 <i>Nucleating agents</i>	42
4.5.2 <i>Fullerene mixtures</i>	45
<b>Chapter 5 - CONCLUDING REMARKS</b>	<b>47</b>
<b>ACKNOWLEDGEMENTS</b>	<b>49</b>
<b>REFERENCES</b>	<b>51</b>



# INTRODUCTION

---

The global demand for energy is increasing. Together with the concerns associated with fossil fuels, this is a problem that has to be solved, or at least partly solved, in the near future. The energy consumption is not increasing all around the world. For example here in Europe the consumption levels are relatively stable and according to predications by the U.S. Energy Information Administration (EIA)<sup>1</sup> these levels will remain likewise over the coming 20 years. The long-term goal is to stop the worldwide increase in energy consumption, which implies that in some parts of the world the energy consumption has to decrease. This will mainly be done by using the produced energy in a more efficient way. The European Union (EU), as well as the individual governments, have put up goals regarding future energy consumption and production. Until 2020, following requirements should be met:<sup>2</sup>

- i) Greenhouse emissions (*i.e.* emissions of carbon dioxide, nitrogen oxides, methane *etc.*) have to be reduced by 20 %.
- ii) 20 % of the energy production should come from renewable energy sources.
- iii) There should be a 20 % improvement of the energy efficiency within the EU.

In addition, the EU has more long-term goals; until 2050, greenhouse emissions should be reduced by 80 % and the energy consumption should be decreased by 30 %. By fulfilling those criteria, the goal is to limit the global temperature increase to 2 °C. The governments of the five Nordic countries have stated even higher goals for their own countries, with a long-term goal of reducing the greenhouse emissions by 85 %.<sup>3,4</sup>

The need for more sustainable energy sources has become an urgent dilemma. In this context, “sustainable” has a double meaning; these energy sources should be

renewable as well as carbon dioxide neutral, *i.e.* they should not increase the amount of greenhouse gases in the atmosphere. This category of desired energy sources includes: wind power, hydroelectric power, wave power, biomass-based energy, geothermal energy and sun energy. Biomass-based energy as well as wind and hydroelectric power are already well developed in the Nordic countries but fossil fuels are still important for the electricity production in both Finland and Denmark.<sup>4</sup>

The sun provides the Earth with more energy than the population needs. If it was possible to utilise a larger part of this energy than we do today, it could partially solve the problems we are facing. Solar cells of different technologies have gained a lot of interest during the last decades. The most commonly used solar cell technology is silicon based. Due to the earlier high prices and long energy payback times of these solar cells, considerable research efforts have been put into the development of alternative solar cell technologies and large improvements have been achieved in the last 10-20 years.

Organic thin-film solar cell technologies, *e.g.* dye-sensitized solar cells and polymer solar cells (PSCs), have gained a lot of interest and have shown to be a promising alternative to their silicon-based counterpart. PSCs normally consist of a blend of a conjugated polymer acting as the light absorber as well as electron donor and a second material, most often a fullerene derivative, acting as electron acceptor. This type of solar cells is the topic of this thesis.

The research efforts within the field of PSCs have resulted in efficiencies of lab-scale devices approaching  $\sim 9-10\%$ , for single layer solar cells.<sup>5,6</sup> This is still lower than the efficiency of silicon-based solar cells, but PSCs have the potential to provide cheaper production and also mechanically flexible devices. One important aspect that needs to be addressed is the relatively low stability and short lifetime of PSCs. Device stability has to be ensured if PSCs should be a competitive alternative to the silicon based solar cells and to other energy sources.

## Introduction

This thesis aims provide a better understanding of the stability of PSCs. The light stability of the polymers as well as the thermal stability of the active layers has been studied. The outline of the thesis is as follows: Chapter 2 introduces PSCs in general. The light stability of the materials within the active layer is discussed in Chapter 3 as well as in Paper I. Subsequently, the thermal stability of the active layer blend is discussed in Chapter 4 together with Paper II-VI. Finally, Chapter 5 will provide concluding remarks.

The work was financed by the Swedish Research Council through the Linnaeus Centre for Bioinspired Supramolecular Function and Design (SUPRA). Electron microscopy was carried out in collaboration with Eva Olsson's group at the Department of Applied Physics, Chalmers University of Technology. Devices were fabricated and characterized in collaboration with the group of Olle Inganäs at the Department of Physics, Chemistry and Biology (IFM), Linköping University.





Chapter 2

## **POLYMER SOLAR CELLS**

---

This chapter provides a general description of the working principles of polymer solar cells (PSCs).

### **2.1 Background**

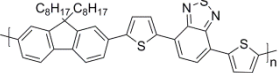
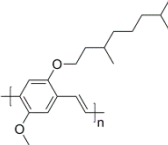
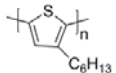
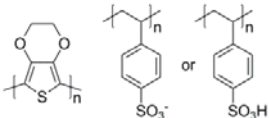
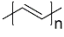
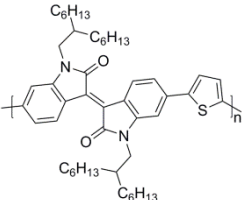
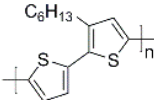
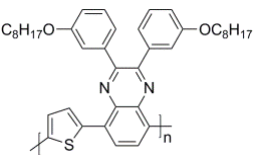
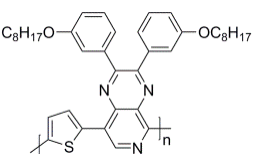
The active layer of PSCs comprises one electron donating and one electron accepting material, of which at least the donor material is a semi-conducting polymer. Most often, the acceptor material is a small molecule, *e.g.* a fullerene derivative, but it can also be another conjugated polymer or a semi-conducting metal oxide.<sup>7-9</sup> The latter case is usually referred to as hybrid solar cells.

Other organic solar cells technologies use small organic molecules as donor materials. An early organic photovoltaic was made from anthracene in 1959 by Kallmann and Pope.<sup>10</sup> Today, solution processed small-molecule solar cells give efficiencies of to  $\sim 7\%$ ,<sup>11</sup> which can be compared with the efficiency of  $\sim 9-10\%$  achieved with PSCs.<sup>5,6</sup> In addition, dye-sensitized solar cells use organic compounds for light absorption, and they are reaching efficiencies up to  $\sim 11\%$ .<sup>12</sup>

### **2.2 Conjugated polymers**

Polymers used for solar cell applications comprise a fully conjugated backbone with alternating single and double bonds. The simplest example is poly(acetylene) (Table 2.1).<sup>13</sup>

Table 2.1: Conjugated polymers mentioned within this thesis.

Polymer	Chemical Structure
APFO-3	
MDMO-PPV	
P3HT	
PEDOT:PSS	
Poly(acetylene)	
PTI-1	
THT	
TQ1	
TQN	

The alternation of single and double bonds enables delocalisation of electrons across the polymer backbone, due to overlap of p-orbitals. The resulting semiconductor comprises a highest occupied molecular orbital (HOMO) and a lowest unoccupied molecular orbital (LUMO). The difference between these energy levels defines the band gap of the material and determines the minimum energy needed to excite an electron. Conducting materials, *e.g.* metals, do not possess a band gap since there is no or only a small energetic difference between the valence and the conduction band. For an insulating material this difference between the energy levels is large and it is therefore more difficult to excite the electrons from HOMO to LUMO. A semi-conductor behaves like an insulator in its neutral state, but via doping the material become an electrical conductor.<sup>14</sup> For poly(acetylene) this can be done with halogen vapours as shown by Shirakawa *et al.* in 1977.<sup>15</sup>

Considerable research efforts have been put into the design of polymers for solar cell applications. The polymers that are developed today comprise more complicated chemical structures than that of poly(acetylene). Poly(acetylene) shows poor solubility in organic solvents and therefore the processability is limited.<sup>16,17</sup> Many conjugated polymers are based on aromatic units, which allows for easy chemical modification and thereby easy alteration of various properties such as processability, opto-electronic properties and stability. The simplest polymer with an aromatic backbone is poly(paraphenylene) (PPP, see figure 2.1). Aromatic polymers have two resonance forms, *i.e.* the aromatic and the quinoid form, that provide a good description of the polymer structure. To achieve the smallest possible band gap, both resonance structures should describe the polymer equally good. In that case, the bond-length difference between single and the double bonds is as small as possible. Most often the aromatic structure is the one describing the polymer the best. To stabilise the quinoid form, donor (D) and acceptor (A) moieties are co-polymerised, forming a so-called DA-polymer.<sup>18</sup>

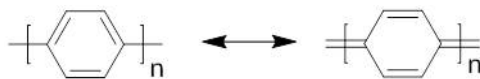


Figure 2.1: Chemical structure of poly(paraphenylene);aromatic (left) and quinoid form (right)

Even small variations in the chemical structure usually change several properties at once.<sup>19</sup> The chemical structure of the polymers can be divided into two parts; *i.e.* the conjugated backbone and the side-chains. Both parts can be chemically modified to achieve desired properties. Examples of properties that could be influenced via such structural changes are listed here below:

- *The band gap* - a smaller band gap offers a better overlap with the solar spectrum and thus higher photon absorption. The polymer absorbs most of the light in the active layer so it is of high importance for the device performance that the polymers comprise broad absorption spectra.
- *The energy levels* - the polymer energy levels should not only be altered to cover a broader part of the solar spectrum, they should also match the energy levels of the acceptor material to guarantee a high potential difference during charge separation. Energy levels are also important for the photo-oxidative stability of the polymers.
- *The solubility* - to improve the polymer solubility in common organic solvents, long alkyl side-chains are introduced. Side-chains will not only influence the interactions with the solvent, but also the interactions with acceptor molecules and thereby influence the nanostructure. The solubility is a crucial factor for solution processing but on the other hand, the introduction of side chains can affect the photo-oxidative stability negatively.

Another property of the polymer that is important for the device performance as well as the processability of the polymer is the *molecular weight*. A higher molecular weight can give rise to higher device efficiencies, but it also means that the polymer will be less soluble.<sup>20, 21</sup> Different molecular weights of the same

polymer will show variations in the absorbance spectra due to differences in aggregation of the polymer chains. Aggregation of polymer chains will also increase the hole mobility polymer resulting in a higher device efficiency. Connected to the molecular weight, band gap and backbone planarity another term is often used: *conjugation length*. Torsion of polymer chains results in saturation of the effective conjugation length with increasing degree of polymerisation.<sup>21</sup>

To absorb more photons, one goal is to make the polymers as black as possible, since that means that a larger amount of photons is absorbed. This could for example be achieved via incorporation of an additional monomer that absorbs light at wavelengths where the original polymer lacks in absorption.<sup>22</sup>

The polymer crystallinity can vary, ranging from completely disordered, *i.e.* amorphous, to semi-crystalline with varying crystallinity. Two often used polymers for solar cell devices are poly(3-hexylthiophene) (P3HT) and poly((9,9-dioctylfluorenyl-2,7-diyl)-*alt*-5,5-(4',7'-di-2-thienyl-2',1',3' -benzothiadiazole)) (APFO-3). These examples represent different classes of polymers where the former is a semi-crystalline polymer and the latter is an amorphous polymer.

In the manuscripts included in this thesis, mainly a quinoxaline-thiophene based polymer (TQ1, Table 2.1) is used. Devices based on this polymer offers promising efficiencies up to  $\sim 6-7\%$ <sup>23,24</sup> and it can be easily synthesised, which is critical for up scaling. Hence, TQ1 is a good choice for large-scale production of PSCs.

### 2.3 Fullerene derivatives

Fullerenes have excellent electron accepting and transporting properties, which makes them a suitable acceptor material in PSCs. Due to the limited solubility of C<sub>60</sub> as well as C<sub>70</sub>, functionalised derivatives have been developed.<sup>25</sup> Most frequently used are [6,6]-phenyl-C<sub>61</sub>-butyric acid methyl ester (PC<sub>61</sub>BM<sup>25</sup>) and [6,6]-phenyl-C<sub>71</sub>-butyric acid methyl ester (PC<sub>71</sub>BM<sup>26</sup>) (Figure 2.2). Besides PCBM, there are several other fullerene derivatives that have been tested for solar

cell applications, such as bis-PCBM<sup>27, 28</sup> (with two functionalising side chains instead of one) and indene-C<sub>60</sub> bisadduct (ICBA).<sup>29</sup>

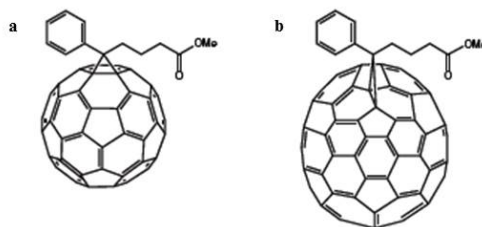


Figure 2.2: Chemical structures of (a) PC<sub>61</sub>BM and (b) PC<sub>71</sub>BM

PC<sub>61</sub>BM and PC<sub>71</sub>BM have different shapes because of a different amount of carbon atoms that comprise the cage. PC<sub>71</sub>BM has a broader spectrum than PC<sub>61</sub>BM (Figure 2.3), which in some cases can increase the device efficiency due to a larger number absorbed photons.<sup>26</sup> On the other hand, PC<sub>61</sub>BM shows better miscibility with some conjugated polymers and a finer and more homogenous nanostructure can therefore be achieved.<sup>30</sup>

Fullerenes and their derivatives can crystallise. In thin films together with a polymer, the crystals can grow several micrometres long after prolonged annealing, which negatively affect the performance of solar cells,<sup>31-33</sup> as will be further discussed in Chapter 4.

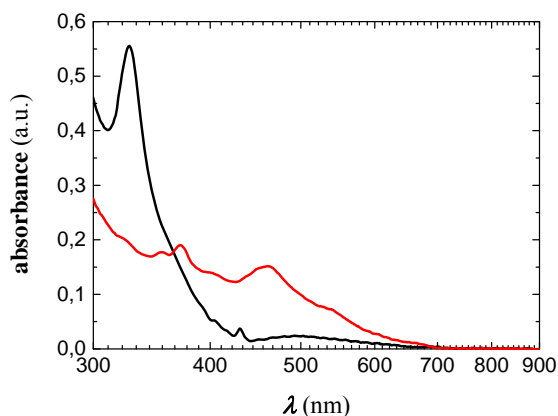


Figure 2.3: UV-Vis spectra of PC<sub>61</sub>BM (black) and PC<sub>71</sub>BM (red) in CHCl<sub>3</sub>

## 2.4 Bulk-heterojunctions

Various active layer architectures have been explored since the introduction of PSCs (Figure 2.4). The first reported PSC was based on a single layer of poly(acetylene), which showed a very low device efficiency.<sup>34</sup> The introduction of a bi-layer architecture significantly improved the device performance.<sup>35,36</sup> Today, the most commonly used architecture is the so-called bulk-heterojunction (BHJ), where the two components are intimately mixed in one layer. The first BHJs were presented by the groups of Friend<sup>8</sup> (polymer-polymer solar cells) and Heeger<sup>37</sup> (polymer-fullerene solar cells) almost simultaneously in 1995, and it has been shown to be superior to earlier architectures. Compared to the bi-layer architecture, the BHJ provides a larger interfacial area between the donor and the acceptor material, which is beneficial for the formation of the charge-transfer state (CT-state) as well as charge separation (see Section 2.7).



Figure 2.4: Schematics of examples of different solar cell architectures; (a) single layer (b) bilayer and (c) BHJ

The BHJ must comprise polymer- and PCBM-rich pathways, allowing electron and hole transport to the electrodes (Figure 2.5). Formation of islands or dead ends of either phase will result in a decrease of the overall conductivity. Phase purity can only be achieved if the compounds crystallise strongly, which rarely is the case for high-performance PSC materials. Therefore, the phases can be considered to be polymer- and PCBM-rich, respectively.

The nanostructure of the BHJ is very important for the solar cell performance. The appearance is governed by (i) the chemical structure of both, the polymer and fullerenes, and (ii) the processing conditions. The chemical structures influence, for example, the miscibility of the materials as well as their crystallinity. Changing

the chemical structure may change the nanostructure due to altered interaction between the donor and acceptor material.<sup>19</sup> By varying processing conditions, *e.g.* solvent,<sup>38</sup> solution temperature and type of substrate,<sup>39</sup> large variations of the nanostructure could be achieved. In addition, the nanostructure is not in thermal equilibrium after deposition and can change upon thermal<sup>31,40,41</sup> and solvent annealing.<sup>42,43</sup> This can be used to optimise the devices<sup>44,45</sup> but annealing during fabrication as well as storage and operation can be detrimental for the device performance.<sup>31-33</sup> This will be further discussed in Chapter 4.

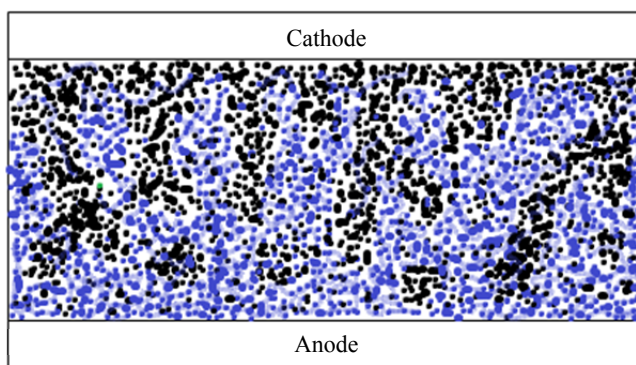


Figure 2.5 Schematic of a BHJ with polymer- (blue) and PCBM-rich (black) phases

## 2.5 Characterisation of the nanostructure

Characterisation of BHJ nanostructures is a key focus of this thesis. Here, the different methods that have been used are listed:

### 2.5.1. Optical microscopy

Structural changes that occur on a length scale larger than 500 nm can be observed with an optical microscope. A light source is used to image the sample, which implies that the resolution is limited by the wavelength of visible light.<sup>46</sup> Cross-polarisers can be used to study anisotropy in thin films of the material and it is commonly used to study both semi-crystalline and liquid-crystalline polymers. Most modern microscopes can operate both with transmitted and reflected light.



The transmission mode provides information about the bulk structure since the light passes through the sample, whereas the reflection mode gives information about the surface and its topography.<sup>47</sup> In this thesis, optical microscopy was mainly used to monitor the crystallisation of PCBM.

### 2.5.2. Atomic force microscopy

The surface composition and topography can be studied by atomic force microscopy (AFM), where phase and height images can be recorded. The phase image can display differences in the surface composition whereas the height image provides information about the topography. In addition, the surface roughness can be measured. An oscillating cantilever is used to image the sample and depending on the interaction between the tip of the cantilever and the different regions of the sample, the strength of oscillations varies. The resolution limit depends on the size of the cantilever tip, which normally has a diameter of several tenths of nanometres. Here, AFM has been used to explore the phase separation in BHJ blends within this thesis.

### 2.5.3. Scanning electron microscopy

In scanning electron microscopy (SEM), an electron beam is used to image the sample, which makes it possible to achieve a higher resolution compared to an optical microscope. The electrons are scattered by the surface of the sample and subsequently collected with different types of detectors, providing different information about the surface. A SEM micrograph can be recorded by either using backscattered or secondary electrons.<sup>46</sup>

To be able to analyse the sample without additional preparation the analysed sample has to be either conducting or semi-conducting, since charges induced by the electron beam have to be transported away from the area that is analysed. Non-conductive samples can be covered by a thin metal layer, allowing imaging of those samples. Within this thesis, most samples have been studied without this

extra layer, which has made it possible to image both, PCBM crystals and phase separation, in BHJ blends.

### 2.5.4. Transmission electron microscopy

Transmission electron microscopy (TEM) image the sample with transmitted electrons, which implies that the sample has to be very thin.<sup>46</sup> The incident electrons will be scattered when passing through a sample: To what extent the electrons will be scattered depends on the density of the different materials. This gives rise to darker and brighter domains in the image. When imaging a BHJ blend, PCBM-rich areas usually appear darker than polymer-rich ones, due to the higher density of PCBM compared to the conjugated polymers.

In addition, electron diffraction patterns can be recorded when analysing a sample with TEM. This provides information about the crystalline nature of the sample. This has been useful within this thesis when studying the crystallisation of PCBM.

### 2.5.5. Spectroscopic methods

Changes of the nanostructure can occur on length scale that is smaller than what microscopic methods permit to monitor. Instead, spectroscopic methods, *e.g.* UV-Vis absorbance or transmittance and in particular photo- and electroluminescence spectroscopy, can be used to detect those changes.

The photoluminescence from the excited state of the polymer is quenched when mixed with PCBM. By monitoring the degree of photoluminescence quenching it is possible to follow small-scale structural changes. Electroluminescence spectroscopy measures the emission energy associated with radiative recombination. A coarser phase separation results in stronger emission from polymer- or PCBM-rich phases, whereas a fine nanostructure gives rise to emission from the CT- state (see Section 2.7).

## 2.6 Device architecture

Lab-scale devices are often prepared on glass substrates, and the different layers are commonly deposited either by spin-coating or by evaporation. The active area of the device is commonly only a few mm<sup>2</sup>, since larger devices often give a lower device performance due to resistive losses in the bottom electrode.<sup>48</sup> There are two main types of devices architectures; the main difference is the direction from which the light enters the devices. Another difference is whether indium tin oxide (ITO) is employed as the anode (normally referred to as the conventional architecture) or the cathode (inverted architecture). An advantage of inverted devices is that they do not require a transparent bottom electrode. Hence, other materials than rather expensive ITO can be used as the bottom electrode material. The layers of the two architectures can be varied in different ways but the following sections describe mainly the devices used in this thesis. A schematic picture of the two architectures is found in Figure 2.6. The conventional type is used for Paper III, V and VI whereas an inverted type is used in Paper I.

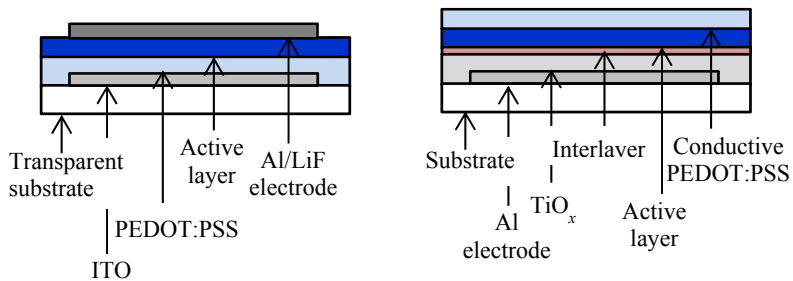


Figure 2.6: Cross-section of a conventional (left) and an inverted (right) device

### 2.5.1. Conventional device architecture

This type is commonly employed for lab-scale solar cell evaluation. For the conventional type, ITO works as the anode. This is deposited on a transparent substrates, such as glass or poly(ethylene terephthalate) (PET) foil. On top of the ITO, a thin layer of poly(3,4-ethylenedioxythiophene):poly(styrenesulfonate) (PEDOT:PSS, Table 2.1) is spin-coated to lower the work function of the

electrode<sup>49</sup> and in addition to make the electrode surface smoother. This material is the most common choice of interlayer, but other compounds have been used successfully, for example molybdenum trioxide ( $\text{MoO}_3$ ).<sup>50,51</sup>

On top of the PEDOT:PSS layer the active layer is deposited. For lab-scale devices, this is usually done by spin-coating due to the simplicity of this method. Other alternatives, such as blade coating, have been implemented since those are more comparable to processes that will be used for large-area, high-throughput printing.

Finally, the cathode is evaporated on top of the active layer. For the devices that are presented in this study the cathode consists of two layers, first a very thin lithium fluoride (LiF) layer, acting as a hole-blocking layer, followed by an aluminium layer. In addition, LiF lowers the work-function of the metal<sup>52</sup> and it can act as a protecting layer during evaporation.

### *2.5.2. Inverted device architecture*

For inverted devices, the bottom electrode can likewise be ITO on top of a transparent substrate, but here it functions as the cathode. For the devices prepared for paper I, ITO was replaced with an aluminium electrode. The electrode is covered with a metal oxide, e.g. titanium oxide ( $\text{TiO}_x$ ) before the active layer is deposited. In addition, an interlayer polymer can be used between the metal oxide and the active layer to increase the efficiency of these solar cells.<sup>53</sup> Finally, the electrode is deposited which can be either modified PEDOT:PSS with a high conductivity or un-modified PEDOT:PSS with a metal electrode on top. Often, a good conductor like silver, arranged in “fingers” to minimise shadowing of the active layer, is used for this purpose.

## 2.7 Working principle of polymer solar cells

This section describes the general working principle of PSCs (Figure 2.7). Within the active layer, part of the incident light is absorbed, mainly by the polymer, if the photon energy is larger than the polymer's band gap. The thickness of the polymer film affects the amount of light that is absorbed; this can be described by the Beer-Lambert law. According to this law, a TQ1 film will need to be  $\sim 80$  nm thick to absorb 50 % of the incident light and  $\sim 270$  nm to absorb 90 % (see Figure 2.8).

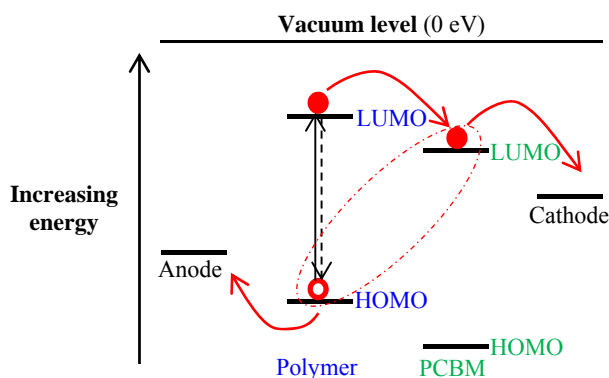


Figure 2.7: Working principle of a polymer solar cell

Upon absorption, an electron is excited from the HOMO to the LUMO of the polymer and a so-called exciton is formed. An exciton is a tightly bound electron-hole pair consisting of an excited electron in LUMO and a hole in HOMO. The exciton diffuses in the polymer-rich phase until it reaches a donor/acceptor interface. The distance that an exciton can diffuse before recombination occurs is usually considered approximately 5-8 nm,<sup>54-56</sup> which means that a donor-acceptor interface should ideally be very close to the molecule where the excitation occurred. This is one reason for the success of the BHJ architecture since the typical dimensions are on the desired length scale. In a well-mixed blend, the donor and the acceptor material are in molecular contact with each other and therefore no diffusion is needed.

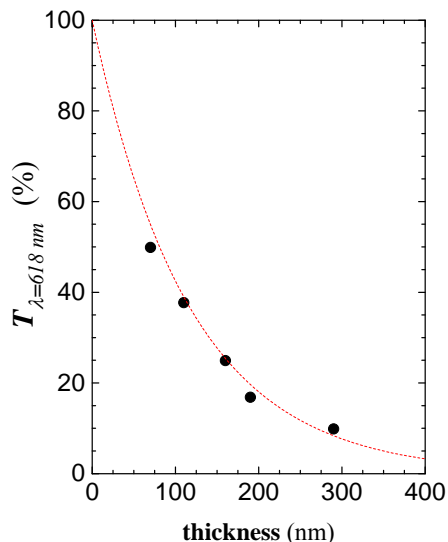


Figure 2.8: Calculated values (dashed line) as well as experimental data (circles) of the transmittance at  $\lambda = 618 \text{ nm}$  as a function of film thickness. Calculations were done using the Beer-Lambert law

When this interface is reached, electron transfer occurs and a CT-state is formed consisting of an electron in the LUMO of the acceptor and a hole in the HOMO of the donor. The CT-state subsequently separates into free charges (charge separation), which are transported to the electrodes (charge transport) where collection of charges occurs. The driving force for the electron transfer is the difference between the LUMO of the donor material and the LUMO of the acceptor material. The latter has to be the lower otherwise it would not be energetically favourable for the electron to leave the donor. Normally a LUMO-LUMO difference of  $\sim 0.3 \text{ eV}$  is required for charge separation, but it has been shown that in some cases an even smaller energy difference is sufficient to achieve high performance solar cells.<sup>57</sup> The charge transport determines the photocurrent, which occurs because of the difference in work function between the two electrodes.

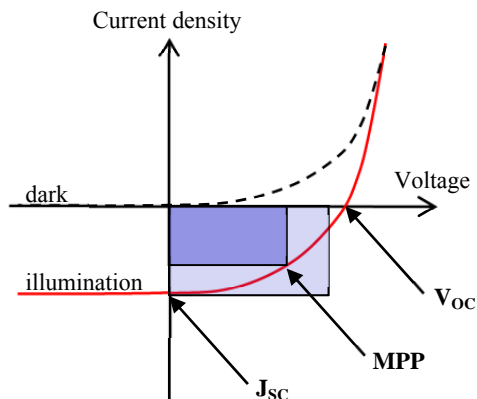


Figure 2.9: Schematic of IV-curves during illumination (solid) and in the dark (dashed)

## 2.8 IV-characteristics

The most common way to evaluate PSCs is to illuminate the device with a solar simulator lamp providing an air-mass (AM) 1.5G spectrum, which resembles the sun spectrum at an inclination angle of  $48.2^\circ$ . This is the incident angle that the sun light has in northern Europe. The lamp intensity that is usually used is called 1 SUN ( $1000 \text{ W m}^{-2}$ ) and it corresponds to the intensity of sunlight during a bright day (no cloud coverage) at zero altitude on Earth.

Upon light absorption, a photocurrent is generated. For evaluation of the devices, this photocurrent is normalised with respect to the device area ( $I$ ) and then plotted against the voltage ( $V$ ), *i.e.* the IV-curve (Figure 2.9). Four different parameters are extracted from this curve and used for device evaluation:

- i) *Short circuit current ( $J_{sc}$ )* - the photocurrent that is achieved when no voltage is applied across the device.
- ii) *Open circuit voltage ( $V_{oc}$ )* - the voltage achieved when the photocurrent is zero. The maximum value is related to the difference between the HOMO of the donor and the LUMO of the acceptor and it can be directly correlated to the energy of the CT-state.<sup>58</sup>

- iii) *Fill factor (FF)* - this is given by the dividing maximum power point (MPP) with the product of  $J_{SC}$  and  $V_{OC}$ .

$$FF = \frac{MPP}{J_{sc}V_{oc}}$$

- iv) *Maximum power point (MPP)* or solar cell efficiency ( $\eta$ ) - this is the maximum power that is achieved ( $P_{max}$ ) divided by the power of the incident light ( $P_{in}$ ). Sometimes MPP is used instead of  $\eta$  to distinguish between lab measurements and certified efficiency measurements.

$$MPP = \eta = \frac{P_{max}}{P_{in}} = \frac{FF * J_{sc} * V_{oc}}{P_{in}}$$

## 2.8 Lifetime and stability of devices

The stability of PSCs has to be ensured before commercialisation becomes feasible. All layers in the sandwich structure can be degraded either physically or chemically. Degradation of the components in the active layer will be discussed from a photo-oxidative perspective in Chapter 3 and from a thermal perspective in Chapter 4. Examples of different degradation mechanisms that are relevant for different components of PSCs (excepted from the active layer) can be degraded are listed below:

- *ITO electrode* - this layer is sensitive to acidic compounds, which will etch the ITO, releasing indium atoms that can diffuse into other layers.<sup>59</sup> For future large scale production the goal is to produce ITO-free devices to remove some of these problems<sup>60</sup> and also to lower the overall cost.
- *PEDOT:PSS* - since this layer is hydroscopic the degradation depends strongly on the humidity.<sup>61</sup> After uptake of water, the PEDOT:PSS



becomes acidic, which is problematic for the ITO electrode as mentioned above.

- *Metal electrode* - the main problem is formation of metal oxides. For example, if aluminium is used then  $\text{Al}_2\text{O}_3$  can form and act as an isolating layer.<sup>62</sup> For inverted devices, this is not relevant since usually silver is used and that less sensitive to water and oxygen.

The sandwich structure of PSCs provides a risk for delamination,<sup>63</sup> leading to a poor contact between the layers. In addition, open edges make it easier for both oxygen and water to enter the device. One way to increase the device stability is encapsulation, which has been proven a very efficient way to protect the device from intrusion of both water and oxygen.<sup>62,64</sup>

### **2.9 Processing techniques for large scale devices**

The polymers and fullerene derivatives used for PSCs are soluble in organic solvents. This is one of the biggest advantages with this technology since continuous, high-throughput printing processes can be applied for solar cell fabrication.<sup>65,66</sup>

Compared to preparation of lab-scale devices, large scale production is normally carried out in ambient conditions.<sup>66</sup> In laboratories, device fabrication can be done under an inert atmosphere where neither moisture nor oxygen is present. In addition, the light illumination can be controlled. Moreover, roll-to-roll processes with a high throughput demand an increased thermal stability of the materials that make up the solar cell. To ensure rapid solvent removal, one or several heating steps are necessary. Usually, temperatures around 140 °C are mentioned when printing on PET foil.<sup>60,62</sup> As will be discussed later in this thesis, these temperatures will normally induce crystallisation as well as phase separation of the BHJ blend. For large scale devices the inverted type has been shown to be the most promising architecture,<sup>60,67</sup> mainly because it does not require any

evaporation steps (*e.g.* for electrode evaporation) and it provides a higher device stability.

## PHOTO-INDUCED DEGRADATION

---

Photo-induced degradation is one of the most prominent degradation mechanisms of the active layer materials. Although not required for all degradation reactions, the presence of oxygen and moisture tends to accelerate this process.<sup>68-70</sup> This chapter will provide a general introduction of the photo-oxidative stability of the active layer components as well as the results from Paper I.

### 3.1 Degradation of the donor polymer

Several factors connected to the chemical structure of the polymer influence its stability. One important aspect is the positions of the HOMO and LUMO levels.<sup>71,72</sup> Energy levels close to vacuum result in a polymer that is less stable towards photo-oxidation. Anthopoulos *et al.* have reported that a LUMO level higher than -4 eV is required for a semi-conductor to be stable against redox reactions.<sup>72</sup>

Apart from the chemical structure of the polymer backbone, it has been shown that the side-chain content with respect to the total molar mass of the polymer plays an important role for the stability of the material.<sup>73</sup> For instance, Ong *et al.* have shown that a higher side-chain content in poly(thiophenes) gives a less stable polymer under ambient conditions.<sup>74</sup> In addition, the stability depends on the chemical structure of the polymer side chains,<sup>75</sup> and the side-chain architecture affects solid-state ordering of the polymer chains and thus diffusion of moisture and oxygen.

Both the backbone and side chains of a polymer can be subjected to degradation. Two of the most widely studied polymers, P3HT and poly(2-methoxy-5-(3',7'-dimethyloctyloxy)-1,4-phenylenevinylene) (MDMO-PPV), show two separate degradation mechanisms, where both parts of the polymer are degraded, originating from the excited state of the polymer.<sup>69</sup>

One of the most noticeable effects of polymer degradation is bleaching, which decreases the amount of absorbed photons and, ultimately, the device efficiency. Bleaching as well as the associated blue-shift in the absorption spectrum<sup>70,76</sup> permit to monitor degradation with a UV-Vis spectrometer.<sup>75,77,78</sup> The absorption spectra of several conjugated polymers, including TQ1, feature two peaks. The peaks are referred to as the high- and the low-energy peak, respectively. The ratio between these peaks ( $A_{max,high-energy\ peak}/A_{max,low-energy\ peak}$ ) depends on the polymer molecular weight (for TQ1, see Figure 3.1).<sup>21,79</sup> By comparing the absorption spectra during degradation it can be seen that this ratio increases upon bleaching, which indicates a reduction in the polymer molecular weight, most likely due to chain scission.

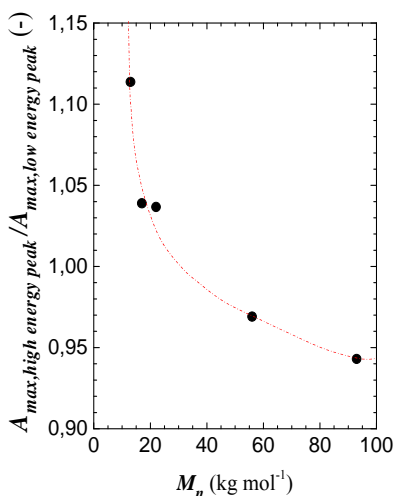


Figure 3.1: The ratio between the high- and low-energy absorption peak as a function  $M_n$  for TQ1 thin films. Red line is a guide to the eye

Reese *et al.* have shown that the decrease in photo-current occurs more rapidly than the decrease in absorbance, which indicates that factors other than bleaching contribute to the loss in solar cell performance.<sup>69</sup> The authors reported a decrease in the yield-mobility products (the product of the yield of free carrier generation per absorbed photon and the sum of the free carrier mobility), which can be

explained with chemical changes of the polymer backbone but also with traps formed due to the oxidation of PCBM.<sup>69</sup>

### 3.2 Degradation of PCBM

The photo-degradation of PCBM is less explored than that of the polymer. Chambon *et al.* have performed a detailed IR study, which indicated that light-induced oxidation predominantly involves the C<sub>60</sub>-cage and not the functionalising side-chain.<sup>80</sup> Reese *et al.* have shown that PCBM oxidation can result in the formation of up to eight distinct products.<sup>69</sup> PCBM degrades more rapidly than the un-substituted C<sub>60</sub>-buckyball, which indicates that modification of the carbon cage decreases its stability, as reported by Anselmo *et al.*<sup>81</sup>

### 3.3 Stability enhancement

#### 3.3.1. PCBM

Compared to the neat polymer, polymer:PCBM blends show superior stability towards photo-oxidative degradation.<sup>69,80</sup> The presence of PCBM quenches the excited state, formed upon light irradiation, and therefore the rate of degradation decreases. In addition, PCBM hinders the degradation that occurs without any light. Reese *et al.* have suggested two explanations: (i) formation of a charge-transfer complex in the ground state and/or (ii) less rapid penetration of oxygen and moisture into more dense active layer films, since the density of PCBM is higher than the density of the polymer.<sup>69</sup> The thermo-oxidative stability of polymers such as MDMO-PPV is also increased when mixed with PCBM due to the radical scavenging properties of the fullerene acceptor.<sup>80</sup>

#### 3.3.2. Polymers with thermo-cleavable side chains

Most donor polymers comprise long side chains to increase the solubility in organic solvents, which facilitates solution-processing of devices. However, side chains have a negative effect on the photo-oxidative stability of the polymer.<sup>73,75-77</sup> Polymers with thermo-cleavable side chains benefit from good solubility during

processing as well as improved stability in the solid state. After deposition of the active layer, the side chains are removed by thermal cleavage, which results in a material that is more resistant towards photo-oxidative degradation.<sup>75,82</sup>

### 3.3.3. *UV-stabilisers*

UV-stabilisers are commonly used to increase the resistance of polymeric materials against UV-irradiation.<sup>83,84</sup> This type of stabilisers consists of UV-absorbing molecules that limit degradation reactions catalysed by UV-light. Although not yet widely employed for PSCs, this kind of UV-stabilizer can potentially be used to increase the photo-stability of the active layer materials.<sup>85</sup>

### 3.3.4. *Encapsulation and protecting layers*

There are two main pathways for oxygen and moisture to enter the device: (i) they are introduced during fabrication or (ii) they enter the device during storage and/or operation. Both, pinholes in, *e.g.*, the metal top electrode as well as unprotected interfaces between partially delaminated device components enable diffusion of oxygen and moisture into the device. Here, appropriate encapsulation can offer good environmental protection and, at the same time, may act as a UV-blocking filter.<sup>62</sup>

Commonly used encapsulation solutions include (i) a top sheet of glass glued to the back substrate or (ii) lamination with different types of plastic foils. In both cases, good sealing of glued/laminated seams is critical.<sup>64</sup> Certainly, lamination is particularly suitable for large-scale production since it can be implemented in a roll-to-roll process.<sup>62</sup>

## 3.4 Photo-oxidative stability of TQ1

As mentioned above, several factors influence the stability, such as the chemical structure of the polymer and the solid-state nanostructure. In addition environmental parameters, *e.g.* temperature and humidity, are critical. Within this thesis and presented in Paper I, bleaching was monitored with a UV-Vis

spectrometer to study the influence of three different parameters on the photo-oxidative stability of TQ1:

- (i) incorporation of a thiophene-hexylthiophene unit
- (ii) molecular weight
- (iii) film thickness.

Carlé *et al.* have reported that the stability of TQ1 is superior compared to other commonly used donor polymers such as P3HT, which was explained by the fact that the thiophene donor unit in TQ1 is not substituted.<sup>73</sup> Replacement of thiophene with a fused thiophene unit resulted in a further improvement in stability due to the high stability of polycyclic structures.

In Paper I the remaining peak absorbance ( $A_{max,remaining}$ ) was used as a measure for the rate of degradation:

$$A_{max,remaining} = \frac{A_{max}}{A_{max,start}} \times 100$$

where  $A_{max}$  is the peak absorbance at any given time and  $A_{max,start}$  is the peak absorbance of the pristine, undegraded sample.

#### 3.4.1 Incorporation of thiophene-hexylthiophene units

It is desirable that the donor polymer strongly absorbs photons at all wavelengths above the band gap, which would result in a black appearance. The absorption spectrum can be modified by incorporation of an additional monomer unit in the backbone,<sup>22</sup> which, however, is likely to influence the stability. In paper I, the photo-oxidative stability of co-polymers comprising a thiophene-hexylthiophene unit in addition to a TQ1 or thiophene-pyrido pyrazine (TQN) motif was studied (Figure 3.2a and 3.2b).

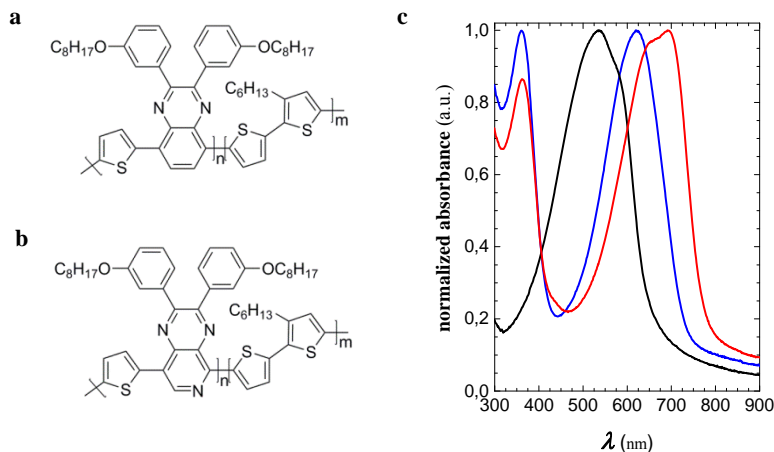


Figure 3.2: Chemical structure of the co-polymers based on (a) quinoxaline ( $m=0$  gives TQ1) and (b) pyrido pyrazine ( $m=0$  gives TQN),  $n=0$  gives THT (c) Normalised absorbance spectra of TQ1 (blue), TQN (red) and THT (black)

Oligothiophenes absorb light wavelengths at which TQ1 and TQN lack in absorption (Figure 3.2c). Therefore, the incorporation of a thiophene-hexylthiophene unit is likely to result in a more black appearance. However, the inferior stability of hexylthiophene-based polymers, as reported by for instance Carlé *et al.*,<sup>73</sup> demands a thorough investigation of the rate of photo-oxidative degradation of TQTHT and TQNTHT.

**Table 3.1:** HOMO and LUMO levels determined by square-wave voltammetry for TQ1 and TQN as well as TQTHT and TPPTHT

Polymer	HOMO (eV)	LUMO (eV)
<b>THT</b>	-5.4	-3.0
<b>TQ1</b>	-5.8	-3.4
<b>TQTHT</b> ( $f_{THT} = 30$ mol%)	-5.6	-3.3
<b>TQTHT</b> ( $f_{THT} = 50$ mol%)	-5.5	-3.2
<b>TQTHT</b> ( $f_{THT} = 80$ mol%)	-5.5	-3.3
<b>TQN</b>	-6.0	-3.7
<b>TQNTHT</b> ( $f_{THT} = 30$ mol%)	-5.9	-3.6
<b>TQNTHT</b> ( $f_{THT} = 50$ mol%)	-5.6	-3.5



The stability study presented in this thesis comprised neat TQ1 and TQN, TQTHTs and TQNTHTs with different fractions of the thiophene-hexylthiophene unit ( $f_{THT}$ ), as well as a thiophene-hexylthiophene polymer (THT, Table 2.1). The decrease of  $A_{max,remaining}$  with time suggests that for TQTHTs the stability decreased with increasing  $f_{THT}$  but is unaffected in case of TQNTHTs (Figure 3.3). Moreover, the bleaching rate of TQN (as well as TQNTHTs) is significantly lower than for TQ1 and TQTHT. This can be explained with the difference in energy levels (Table 3.1), which indicates that the former is likely to be less stable towards oxidation reactions.<sup>71,72</sup>

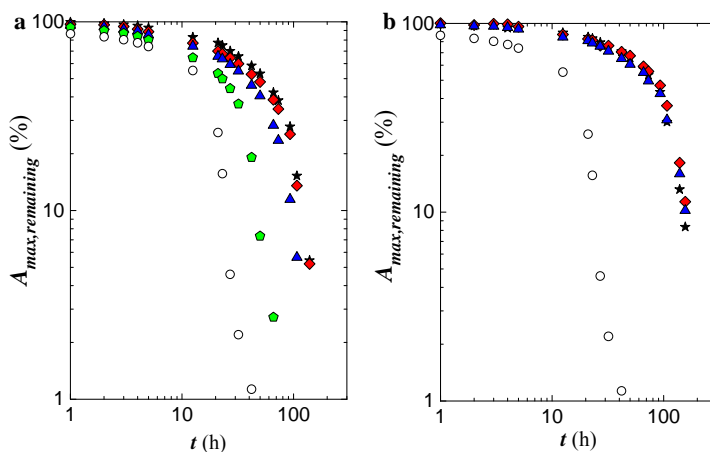


Figure 3.3:  $A_{max,remaining}$  as a function of time for (a) TQTHT and (b) TQNTHT with  $f_{THT} = 0$  mol% (stars), 30 mol% (diamonds), 50 mol% (triangles), 80 mol% (pentagons) and 100 mol% (circles)

### 3.4.2. Influence of molecular weight

The polymer molecular weight can influence the device performance. Usually, a higher molecular weight gives rise to a higher power conversion efficiency.<sup>20</sup> The impact of molecular weight on the photo-oxidative stability is less explored. In Paper I, different molecular weights of TQ1 were tested, but no variation in the stability of this donor polymer was observed.

### 3.4.3. Influence of film thickness

A thicker film consists of more material compared to a thinner film. Thus, it takes a longer time for the thicker film to bleach completely. Accordingly,  $A_{max}$  of thicker TQ1 films, decreases more slowly with time (Figure 3.4a). If the absolute absorbance is used instead of  $A_{max,remaining}$  (Figure 3.4b), it can be seen that the five different curves (corresponding to the five investigated thicknesses) have a similar slope. This indicates that the decrease in absorbance occurs at the same rate, independent of thickness. By calculating the absorbance with the Beer-Lambert law, it is possible to obtain a fair comparison between films of different thickness.

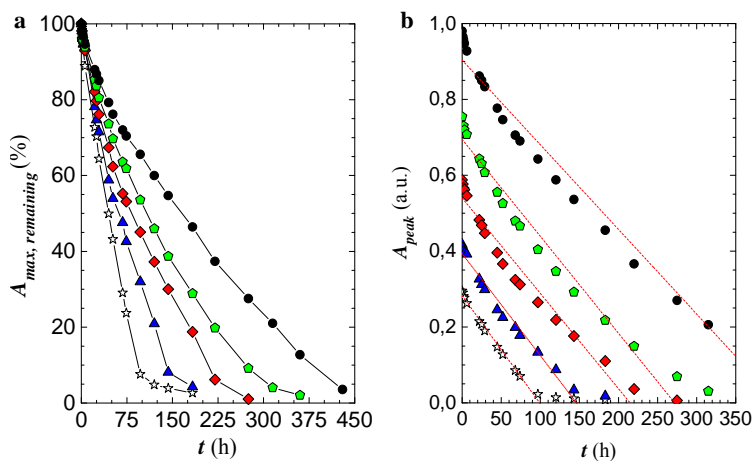


Figure 3.4: (a)  $A_{max,remaining}$  as a function of time for TQ1 films with different thickness. (b) Absolute value of the absorbance of the low energy peak as a function of time. Linear fits of data points are shown as dotted lines. In both (a) and (b) the thickness of the films is 70 nm (stars), 110 nm (triangles), 160 nm (diamonds), 190 nm (pentagons) and 290 nm (circles)

## THERMAL STABILITY OF THE BULK-HETEROJUNCTION BLEND

---

PSCs are subjected to increased temperatures during production and operation. Depending on the type of BHJ blend, thermal treatment can either improve<sup>45,86</sup> or worsen their photovoltaic performance.<sup>31-33</sup> Generally, the nanostructure of BHJs is relatively stable up to the glass transition temperature of the blend ( $T_g^{blend}$ ) but tends to deteriorate if exposed to higher temperatures. Thus, if the processing and/or operating temperature exceed  $T_g^{blend}$ , the thermal stability of the nanostructure has to be improved. The following chapter discusses the thermal stability of BHJ blends as well as several means to improve their temperature resistance.

### 4.1 Background

BHJ blends must be able to withstand elevated temperatures. International standard ASTM E 1171 as well as the ISOS-3 standard<sup>87</sup> proposed by the organic photovoltaics community, demand testing temperatures up to 85 °C for stability measurements of solar cells, which is also a typical operating temperature. In addition, to realise a high throughput production of PSCs, one or several heating steps will be necessary in order to ensure rapid solvent removal.<sup>62</sup> If PET foil substrates are used, the processing temperature is limited to 140 °C. An ITO-covered PET substrate makes up ~ 40-50 % of the total device cost, in contrast to only ~ 20-30 % for the active layer.<sup>88</sup> Thus, alternative but more expensive substrates, such a poly(ethylene naphthalate) (PEN),<sup>60</sup> which can tolerate higher annealing temperatures, would significantly increase the overall cost of the device.

Many BHJ blends are not compatible with elevated production and operation temperatures. Phase separation and crystallisation occur once the blend is heated

above its glass transition temperature. In many cases, this leads to a detrimental decrease in device performance.

#### 4.1.1 Thermal transitions

The thermal behaviour of BHJ nanostructures is governed by material-specific transition temperatures, which for example depend on the chemical structure, polymer molecular weight,<sup>46,47</sup> and thermal history.<sup>89</sup> For the here discussed organic semiconductors the following transition temperatures must be considered:

- *Glass transition temperature ( $T_g$ )* - At this temperature the transition from the glassy state, where the material is 'frozen in', to the rubbery state, where long-range motion becomes possible, occurs. Only amorphous material displays a  $T_g$ . For polymers, just below  $T_g$  local segmental motion can occur, which is referred to as physical ageing. In addition, minor sub-glass transitions (sub- $T_g$ s) can occur below the main  $T_g$ .
- *Melting temperature ( $T_m$ )* – During heating crystalline material melts at  $T_m$ .
- *Liquid-crystalline to isotropic transition temperature ( $T_{LC}$ )* – Some materials including many donor polymers enters a liquid-crystalline state at higher temperatures, which becomes isotropic at  $T_{LC}$ .
- *Crystallisation temperature ( $T_c$ )* – When cooled from the melt amorphous (or liquid-crystalline) material crystallises at  $T_c$ .

Many polymer:fullerene blends display partial miscibility. As a result, the blend transition temperatures can strongly differ from those of the neat components.<sup>40</sup>

#### 4.1.2. Phase separation and fullerene crystallisation in BHJ blends

Above  $T_g$ , phase separation occurs which can be driven by (i) liquid-liquid demixing into larger polymer- and PCBM-rich domains and (ii) crystallisation of either component. For some semi-crystalline polymers such as P3HT, annealing above  $T_g$  can be used to improve the solar cell efficiency<sup>45,86</sup> and in addition, crystallisation of the polymer tends to improve the thermal stability of the blend.<sup>90</sup> For non-crystalline polymers liquid-liquid demixing is the most prominent phase-separation mechanism.

At temperatures higher than  $T_g^{blend}$ , PCBM starts to crystallise. These crystals can reach a size of up to several micrometres, which is detrimental for the device performance.<sup>31,32</sup> PC<sub>61</sub>BM crystals can be formed in blends with semi-crystalline<sup>45,91,92</sup> as well as amorphous polymers.<sup>38, 40</sup> Neat PCBM crystals are hexagonal<sup>93,94</sup> but within a polymer matrix the crystals adopt a disc- or needle-like shape.<sup>31,38,41</sup> Typically, a depletion zone, which consists of more polymer-rich material, surrounds the fullerene crystals.<sup>31,95</sup> Moreover, fullerene crystals tend to protrude from the film surface and can achieve a height of several hundred nanometres even though the film thickness is usually  $\sim 100$  nm.<sup>39</sup>

The thermal stability can be improved by limiting the growth of fullerene crystals. For instance, this can be achieved by (i) using donor polymers with a higher  $T_g^{polymer}$ ,<sup>96</sup> (ii) crosslinking of the polymer<sup>97,98</sup> (iii) addition of a functionalised monomer<sup>99</sup> and (iv) light-soaking, which causes dimerization of PCBM.<sup>70,100,101</sup> Moreover, in complete devices the top electrode to some extent confines PCBM crystallisation.<sup>102</sup>

#### 4.1.3 Determination of thermal transitions

A number of experimental techniques permit to investigate thermal transitions. Those can be divided into different families (examples of techniques are given in brackets): calorimetric (DSC and MTDSC), optical (temperature-variable optical

microscopy), X-ray (GIXS) mechanical (DTMA), spectroscopic (variable-temperature ellipsometry) and electrical methods (DETA). Quoted thermal transitions strongly depend on the measurement technique as exemplified by the range of reported values for the glass transition of PC<sub>61</sub>BM,  $T_g^{PCBM} \sim 110\text{-}150$  °C (Table 4.1).

**Table 4.1:** Methods for determination of thermal transition

Method	Full name	$T_g$ of PC <sub>61</sub> BM (°C)
DSC	Differential Scanning Calorimetry	
MTDSC	Modulated Temperature Differential Scanning Calorimetry	131, <sup>103</sup> 118 <sup>104</sup>
DTMA	Dynamic Thermal Mechanical Analysis	154 <sup>105,*</sup>
DETA	Dielectric Thermal Analysis Variable-Temperature Ellipsometry	111 <sup>40</sup>
GIXS	Grazing incidence X-ray scattering	148 <sup>106,*</sup>

\*Probably onset of PC<sub>61</sub>BM crystallisation

In this thesis, DSC is the principal method that was employed to study the thermal behaviour of both neat materials and blends, due to its ease of use and versatility.

#### 4.1.4 Thermal transitions of materials encountered in this thesis

The work presented in this thesis is based on the polymer TQ1, which features a high  $T_g \sim 100$  °C (measured by variable-temperature ellipsometry) as reported by Kroon *et al.*<sup>107</sup> TQ1 is a non-crystalline polymer but displays a liquid-crystalline transition ( $T_{LC} \sim 300$  °C)<sup>108</sup> that can be detected with both with polarised optical microscopy and with DSC.

PC<sub>61</sub>BM has a  $T_g^{PC_{61}BM} \sim 110\text{-}150$  °C<sup>40,103,106</sup> and a  $T_m \sim 290$  °C.<sup>92</sup> PC<sub>71</sub>BM shows a higher  $T_m \sim 320$  °C<sup>92</sup> which suggest that also the  $T_g$  should be shifted to higher temperatures as compared to PC<sub>61</sub>BM. Often two melting peaks are observed with MTDSC for PC<sub>61</sub>BM,<sup>92,103</sup> which most likely are due to different polymorphs of

the material. An additional third peak has been observed and was assigned to solvent bound in crystalline PC<sub>61</sub>BM.<sup>104</sup>

The PC<sub>61</sub>BM melting temperature of 1:1 TQ1:PCBM is reduced by only  $\Delta T_m \sim 5$  °C compared to neat PC<sub>61</sub>BM.<sup>41</sup> Other blends such as 1:1 P3HT:PCBM and 1:1 APFO-3:PC<sub>61</sub>BM show significantly higher melting point depressions of  $\Delta T_m \sim 80$  °C<sup>92,103</sup> and  $\Delta T_m \sim 30$  °C,<sup>40</sup> respectively. This suggests that the miscibility of PC<sub>61</sub>BM in TQ1 is relatively low. Hence, this blend should in principle show two  $T_g$ s, which are, however, difficult to resolve since  $T_g^{PC_{61}BM} \sim T_g^{TQ1}$ .

The schematic thermometer displayed in Figure 4.1 summarises the thermal transitions of this blend with respect to the likely processing and operating temperatures of 85 °C and 140 °C.

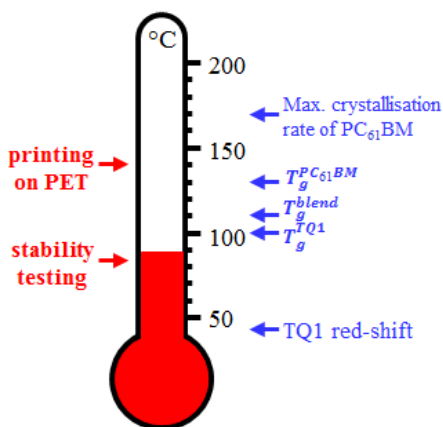


Figure 4.1: Thermometer correlating processing and operating temperatures to critical transition temperatures: maximum crystallisation rate of PC<sub>61</sub>BM and  $T_g^{blend}$  (cf. Paper IV),  $T_g^{PC_{61}BM}$  (cf. ref. 103),  $T_g^{TQ1}$  (cf. ref. 107) and TQ1 red-shift (cf. Paper III)

#### 4.2 Using the onset of PC<sub>61</sub>BM crystallisation to determine the upper limit of the glass transition temperature

Paper II presents a method based on UV-Vis spectroscopy that permits to determine the upper limit of  $T_g^{blend}$  of TQ1:PC<sub>61</sub>BM films, which has not been possible to detect with ellipsometry or DSC. This technique exploits the fact that PCBM crystals, which only grow above  $T_g^{blend}$ , scatter light.<sup>96</sup> By monitoring the

amount of scattered light as a function of temperature, it is possible to measure the  $T_g$  for thin film geometries. The incident light ( $I_0$ ) is divided into scattered ( $I_{scattered}$ ), transmitted ( $I_{transmitted}$ ) and reflected light ( $I_{reflected}$ ) when passing through a sample in a UV-Vis spectrometer (Figure 4.2).

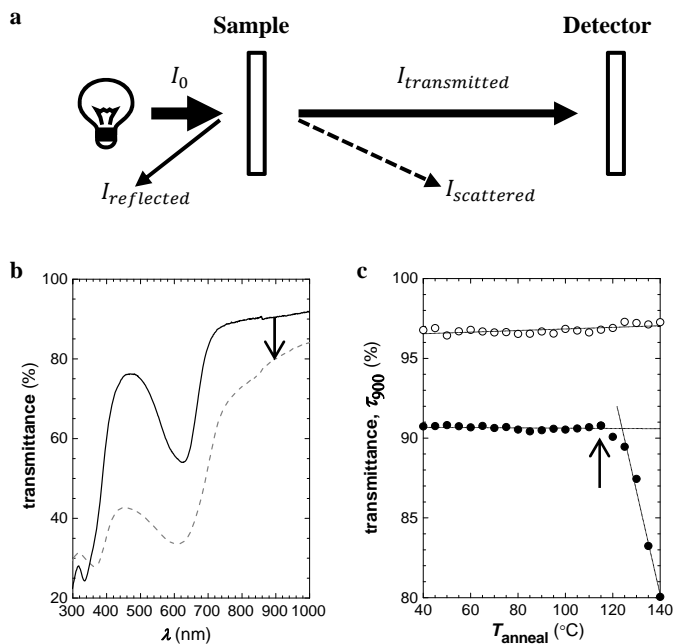


Figure 4.2: (a) Schematic of incident light ( $I_0$ ), reflected light ( $I_{reflected}$ ), scattered light ( $I_{scattered}$ ) and transmitted light ( $I_{transmitted}$ ) during measurement of a UV-Vis transmittance spectrum (b) UV-Vis transmittance spectra of pristine, spin-coated (solid) and annealed (dashed) 1:1 TQ1<sub>56k</sub>:PC<sub>61</sub>BM. Arrows mark the change in transmittance at 900 nm (c) transmittance at  $\lambda = 900$  nm for TQ1<sub>56k</sub> (open circles) and TQ1<sub>56k</sub>:PC<sub>61</sub>BM (filled circles) as a function of annealing temperature  $T_{anneal}$ . Dashed lines represent linear fits. Arrows mark the onset of PCBM crystallisation

Formation of PC<sub>61</sub>BM crystals increases  $I_{scattered}$  and thereby  $I_{transmitted}$  is decreased. This can be seen by comparing the transmittance spectra recorded before and after annealing of a 1:1 TQ1:PC<sub>61</sub>BM film (Figure 4.2b). By monitoring the transmittance as a function of temperature, it was possible to detect the onset of PC<sub>61</sub>BM crystallisation (figure 4.2c). This is done at a wavelength where TQ1 is transparent, e.g.  $\lambda = 900$  nm, so that changes in the transmittance



spectra can be unambiguously assigned to light scattering from PC<sub>61</sub>BM crystals. The here proposed method is sensitive to light scattering from fullerene crystals that are at least  $\sim 0.5 \mu\text{m}$  large, which prevents studying the onset of the  $T_g$ .

The upper limit of  $T_g$  was determined for TQ1:PC<sub>61</sub>BM blends based on two TQ1 batches with different molecular weight ( $M_n \sim 12$  or  $56 \text{ kg mol}^{-1}$ ). Similar to other conjugated polymers,<sup>21</sup> the higher molecular-weight TQ1 displayed a  $10 \text{ }^\circ\text{C}$  higher  $T_g$  (Table 4.2). In addition, the upper limit of the  $T_g$  was determined for blends based on TQN, with a  $T_g \sim 46 \text{ }^\circ\text{C}$  for the neat polymer (determined with temperature variable ellipsometry),<sup>51</sup> which is low as compared to neat PC<sub>61</sub>BM, and for a semi-crystalline polymer, PTI-1 (for chemical structures see Table 2.1 and for light scattering results see Table 4.2).

**Table 4.2:** Onset of PC<sub>61</sub>BM crystallisation determined by UV-Vis

Blend	$T_c^{PC_{61}BM}$ ( $^\circ\text{C}$ )
1:1 TQ1 <sub>12k</sub> :PC <sub>61</sub> BM	105
1:1 TQ1 <sub>56k</sub> :PC <sub>61</sub> BM	115
1:1 TQN:PC <sub>61</sub> BM	85
1:1 PTI-1:PC <sub>61</sub> BM	145

#### 4.3 Annealing of TQ1:PC61BM films below the glass transition temperature

Solution-processed BHJs tend to adopt a nanostructure that is not in thermodynamic equilibrium, but can be preserved as long as the material is kept at temperatures much lower than  $T_g^{blend}$ . However, as discussed in Paper III, mild annealing of TQ1:PC<sub>61</sub>BM blends close to  $T_g^{blend}$  can induce local conformational changes of the donor polymer. The associated changes in nanostructure cannot be detected with microscopic techniques, such as TEM and AFM, which indicates that they occur on a length scale much smaller than  $10 \text{ nm}$  (Figure 4.3).

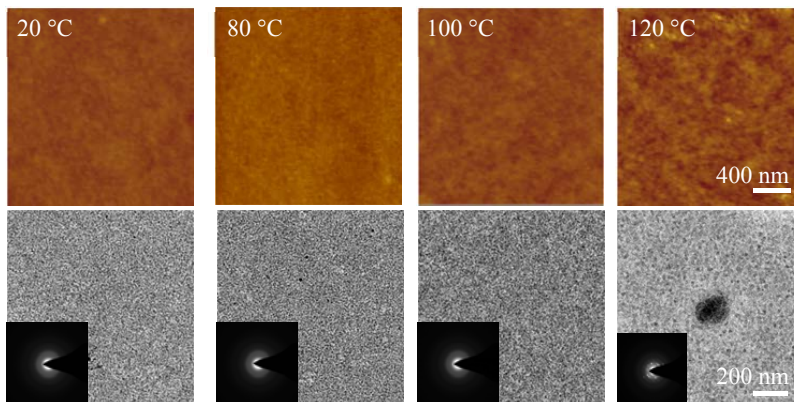


Figure 4.3: AFM images (upper row), TEM images (lower row) and electron diffraction patterns (lower row, insets) of 1:1 TQ1:PC<sub>61</sub>BM thin films after annealing for 10 min at the indicated temperatures

In contrast, UV-Vis absorption measurements indicate that local conformational changes do indeed occur during annealing at temperatures as much as 65 °C below  $T_g^{blend}$  (Figure 4.4). Upon annealing the absorbance, as well as the photoluminescence and electroluminescence spectra, of the blend redshift. This can be caused by (i) an increase in conjugation length and (ii) local aggregation of TQ1, which would require partial diffusion of PC<sub>61</sub>BM.

Local conformational changes that occur upon mild annealing of TQ1:PC<sub>61</sub>BM blends could be correlated with the thermal behaviour of complete solar cells. Mild annealing below  $T_g$  resulted in an increase in power conversion efficiency whereas annealing above  $T_g$  was detrimental for the device performance (Figure 4.5). In addition, lateral variations in photocurrent decreased when the active layer was annealed at temperatures approaching  $T_g$ . This is evidenced by a smaller standard deviation of the recorded device efficiencies, which are based on four cells on the same substrate (*cf.* ‘error bars’ in Figure 4.5). Hou *et al.* have reported that the device performance can vary by up to ~ 30 % across the same substrate, which was explained by lateral variations in the nanostructure.<sup>109</sup> Hence, a smaller spread

in device efficiencies suggests that the film has become more homogenous over the substrate area.

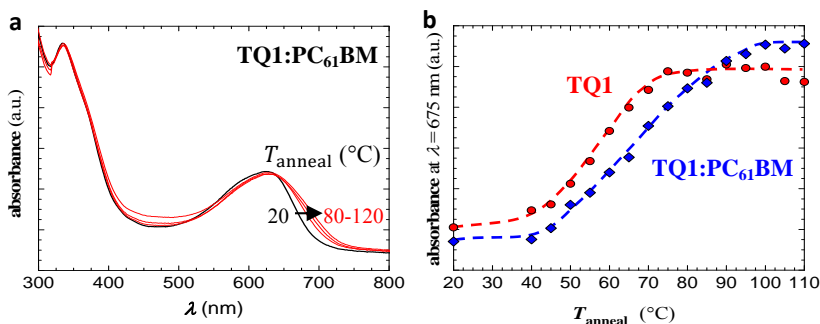


Figure 4.4: (a) UV-Vis absorbance spectra of a spin-coated 1:1 TQ1:PC<sub>61</sub>BM thin film (black) that has been stepwise annealed for 5 min every 5 °C up to 80 °C, 100 °C and 120 °C (red). Note the distinct red-shift upon annealing (black arrow) (b) UV-Vis absorbance at  $\lambda = 675$  nm as a function of annealing temperature of a TQ1 (red circles) and 1:1 TQ1:PCBM thin film (blue diamonds)

#### 4.4 Annealing of TQ1:PC<sub>61</sub>BM films above glass transition temperature

Annealing at temperatures higher than  $T_g^{blend}$  is detrimental for TQ1:PC<sub>61</sub>BM devices (Figure 4.5). This is probably due to both, rapid coarsening of the nanostructure as well as crystallisation of PC<sub>61</sub>BM, which occur upon annealing above  $T_g^{blend}$ . In order to achieve a better understanding of the crystallisation dynamics, the kinetics of PC<sub>61</sub>BM crystallisation were studied in more detail (Paper IV). Two processes, *i.e.* nucleation and growth, govern the crystallisation.

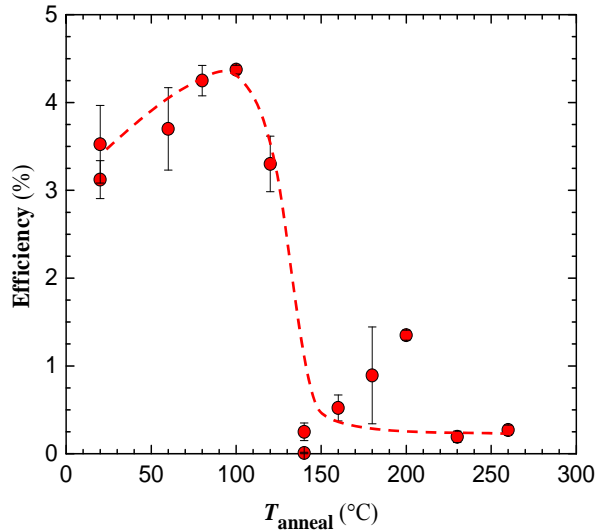


Figure 4.5: Solar cell device efficiency as a function of annealing temperature  $T_{\text{anneal}}$  of the TQ1:PC<sub>61</sub>BM active layer. Error bars indicate the standard deviation of 4 devices on the same substrate. Red dashed lines are a guide to the eye

Nucleation initiates crystallisation. In order for a crystal to start growing, a stable nucleus must form, which requires a critical nucleus size.<sup>110, 111</sup> Nucleation can be either homogenous or heterogeneous. Homogenous nucleation occurs in very pure materials and does not involve foreign substances. Heterogeneous nucleation implies that nucleation initiates with help of a foreign substance, such as an impurity or a surface. Stable nuclei continue to grow, which can be either interface- or diffusion controlled.<sup>110,111</sup> Provided that the composition around the crystals is unchanged during the growth process, the growth is governed by reorganisation at the liquid-interface, *i.e.* it is interface controlled. In contrast, diffusion controlled growth is governed by the diffusion rate of the crystallising material since there is a composition gradient across the volume closest to the crystal growth front due to depletion.

## Thermal stability of the bulk heterjunction blend

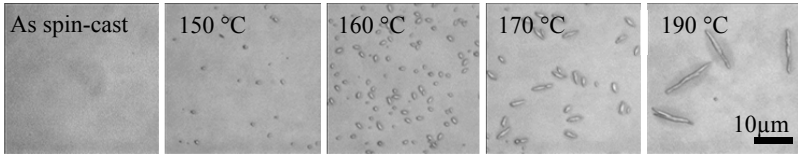


Figure 4.6: Optical micrographs of 1:1 TQ1:PC<sub>61</sub>BM thin films spin-coated on glass, annealed 3 min at indicated temperatures

In this thesis, crystallisation kinetics of PC<sub>61</sub>BM crystallisation were studied for 1:1 (by weight) TQ1:PC<sub>61</sub>BM thin films by means of isothermal annealing at temperatures between  $T = 110\text{ °C}$  ( $\sim T_g^{blend}$ , determined by the light scattering method; *cf.* Section 4.2) and  $T = 230\text{ °C}$ . Both, the size and amount of crystals was shown to be temperature dependent (Figure 4.6).

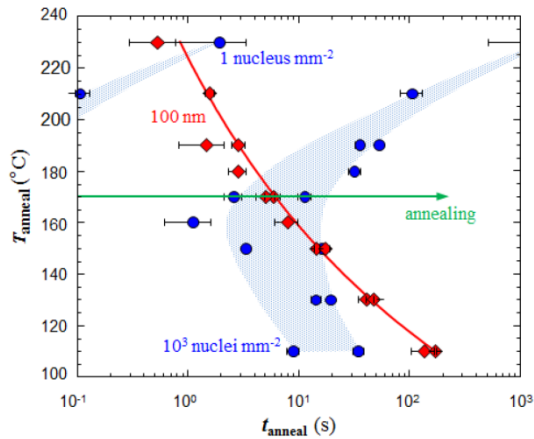


Figure 4.7: Time-temperature-transformation (TTT), indicating the progress in nucleation (blue) and growth (red). Green arrow corresponds to isothermal annealing at 170 °C

Careful analysis of optical micrographs, recorded after discrete annealing steps at gradually increasing temperatures, permitted to determine growth- and nucleation rates. Since the crystal width reached a constant value already after the first annealing step, the growth rate was compared to changes in the crystal length. In addition, to ensure that no smaller crystals were present after annealing at lower temperatures, SEM and TEM were carried out. To illustrate the relative

contribution from crystal nucleation and growth, we constructed a time-temperature-transformation (TTT) diagram (see Figure 4.7). The TTT diagram suggests that low nucleation rate limits PCBM crystallisation, which inevitably results in the growth of micrometre-large PC<sub>61</sub>BM crystals.

#### **4.5 Improving the thermal stability of TQ1:PC<sub>61</sub>BM blends**




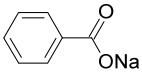
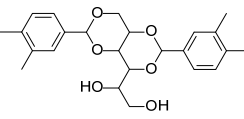
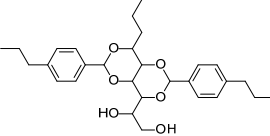
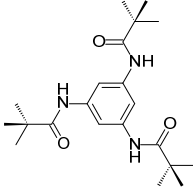
As mention above, several methods exist to permit to improve the thermal stability of the nanostructure. Paper V and VI introduce two additional routes that be used to prepare more stable BHJ blends.

##### *4.5.1 Nucleating agents*

Nucleating agents have been used in polymer technology for a long time since they are able to create desired properties for certain applications, for example to clarify isotactic polypropylene.<sup>112-114</sup> Recently, nucleation agents have been explored also for conjugated polymers as well as other semi-conductors for organic electronics applications.<sup>115</sup> In addition, Richards *et al.* reported that addition of the un-substituted C<sub>60</sub>-fullerene affects the number and the size of PC<sub>61</sub>BM crystals in a P3HT matrix.<sup>116</sup>

By introduction of a nucleating agent, a heterogeneous nucleation site is added, which initiates crystallisation. Since it was shown in Paper III that a low rate of nucleation limits PC<sub>61</sub>BM crystallisation, nucleating agents can help to significantly increase the nucleation rate and thereby strongly reduce the crystal size.

**Table 4.3:** Chemical structure of nucleating agents, increase in peak crystallisation temperature  $\Delta T_c^{nuc}$  of TQ1:PC<sub>61</sub>BM containing 2 wt% nucleating agent with respect to PC<sub>61</sub>BM and nucleating efficiency *NE*.

nucleating agent	chemical structure	$\Delta T_c^{nuc}$ (°C)	Nucleating Efficiency (%)
<b>C<sub>60</sub></b>		9	26
<b>C<sub>70</sub></b>		0, 6	0, 18
<b>SWNT</b>		0, 13, 24	0, 38, 71
<b>NaBz</b>		0, 14, 33	0, 41, 97
<b>NaBz*</b>		8, 17	24, 50
<b>DMDBS</b>		7	21
<b>TBPMN</b>		4	12
<b>BTA</b>		1	3

A number of compounds were tested for their ability to nucleate PC<sub>61</sub>BM (see Table 4.3). To this end,  $T_C^{PC_{61}BM}$  and  $T_C^{max}$ , which correspond to the PC<sub>61</sub>BM crystallisation temperature in the blend and the highest crystallisation temperature of optimally self-seeded neat PC<sub>61</sub>BM, respectively, were extracted from DSC cooling thermograms (Figure 4.8a). Based on these measurements, the nucleating efficiency of the investigated compounds could be calculated (*cf.* Paper IV), which was particularly high for Sodium Benzoate (NaBz) and single walled carbon nanotubes (SWNT) with 97 and 71 %, respectively. However, both compounds gave rise to several crystallisation exotherms, which indicate inhomogeneous mixtures. In contrast, from DSC measurements as well as optical microscopy it could be concluded that in particular un-substituted C<sub>60</sub>-fullerene is not only an efficient nucleating agent but also gives rise to homogeneous mixtures (see Figure 4.8b). Therefore, the use of C<sub>60</sub> as a nucleating agent was studied in more detail.

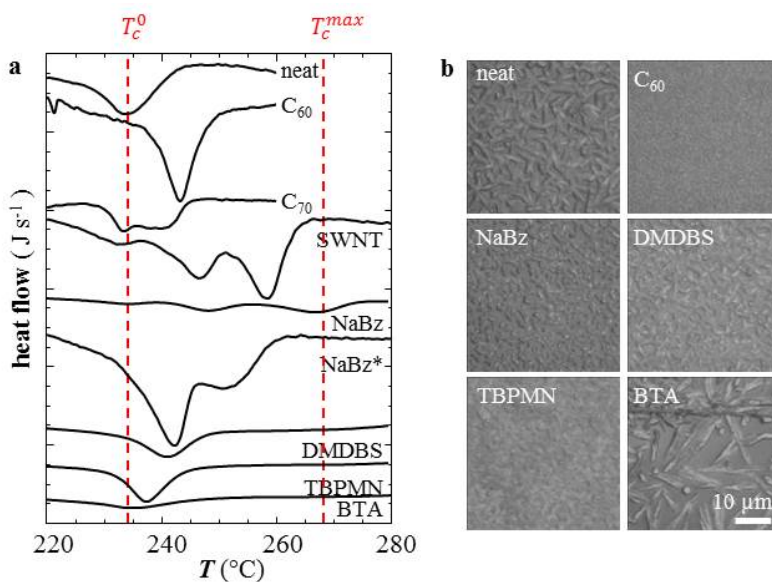


Figure 4.8: (a) DSC cooling thermograms of 1:1 TQ1: PC<sub>61</sub>BM with 2 wt% of the indicated nucleating agents (3 wt% for SWNT) (b) micrographs of 1:1 TQ1: PC<sub>61</sub>BM with 2 wt% of the indicated nucleating agents



The effect of using  $C_{60}$  as a nucleating agent was studied by several complementary microscope techniques, *i.e.* optical microscopy, SEM and TEM. Both, the crystal amount and the size, could be controlled by adding different amounts of  $C_{60}$  to 1:1 TQ1:PC<sub>61</sub>BM blends. Remarkably, devices based on  $C_{60}$ -nucleated active layers revealed that addition of as small as 5 wt% of  $C_{60}$  significantly improves the thermal stability of the blend nanostructure during annealing at 130 °C (see Figure 4.9). Evidently, careful nucleation of the fullerene acceptor material results in BHJ blends that are more resistant towards annealing above  $T_g^{blend}$ .

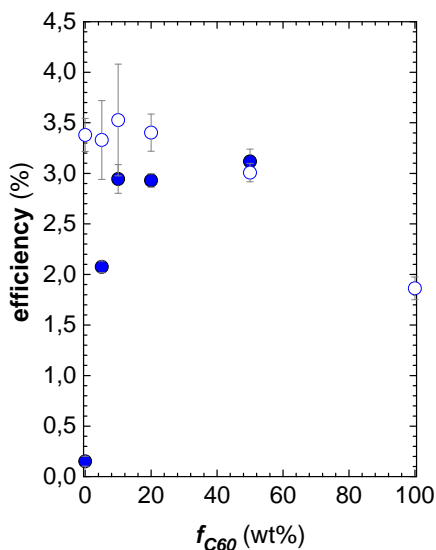


Figure 4.9: Efficiency as a function of  $C_{60}$  fraction for pristine (open symbols) and annealed at 130 °C for 10 min (solid symbols) 1:1 TQ1:fullerene devices

#### 4.5.2 Fullerene mixtures

Fullerene derivatives such as bis-PCBM contain several isotopes, which strongly hinders crystallisation and results in a largely amorphous, glassy material.<sup>117</sup> Recently, fullerene mixtures have been shown to improve the thermal stability due to hindered crystallisation.<sup>118-120</sup> In Paper VI, this tendency of fullerene mixtures to vitrify is exploited to improve the thermal stability of BHJ blends. The two most

widely studied fullerene derivatives, *i.e.* PC<sub>61</sub>BM and PC<sub>71</sub>BM, which itself can form several isotopes, are mixed and blended with TQ1.

DSC analysis, optical microscopy and TEM were used to examine crystallisation of the PC<sub>61</sub>BM:PC<sub>71</sub>BM binary system. From these measurements, it was concluded that crystallisation is prevented in mixtures consisting of 80 wt% PC<sub>61</sub>BM and 20 wt% PC<sub>71</sub>BM. Solar cells based on 5:4:1 TQ1:PC<sub>61</sub>BM:PC<sub>71</sub>BM active layers displayed significantly improved thermal stability compared to TQ1:PC<sub>61</sub>BM reference devices.

**Table 4.4:** Prices of different fullerenes and fullerene mixtures

Type	Price (€g <sup>-1</sup> )
C <sub>60</sub>	15
C <sub>70</sub>	150
PC <sub>61</sub> BM	150
PC <sub>71</sub> BM	780
Mixture of PC <sub>61</sub> BM/PC <sub>71</sub> BM (ratio 80/20)	100

Besides the good thermal stability that is achieved by using PCBM-mixtures a reduction in price of the fullerene material can be anticipated. This is because from the fullerene synthesis a mixture of predominantly C<sub>60</sub> and C<sub>70</sub> is obtained. Hence, by directly using the synthesised fullerene mixture, purification can be avoided which should result in a less expensive product (see prices from Solenne BV for various fullerenes and their derivatives in Table 4.4).

## CONCLUDING REMARKS

---

Polymer solar cells (PSCs) are a promising alternative to silicon-based solar cells since their ease of production, *e.g.* by large-area printing or coating techniques, offers the potential for low cost devices. However, high-throughput roll-to-roll processes demand thermally stable materials because such a process would require one or several heating steps. In addition, during operation the devices have to withstand chemical- and physical degradation. The photo-oxidative and thermal stability of the active layer materials have been the main subjects of this thesis. Most work presented in this thesis focuses on bulk-heterojunction blends of a thiophene-quinoxaline co-polymer (TQ1) and different fullerene derivatives.

The first part of the thesis examined bleaching of TQ1 as well as a thiophene-pyrido pyrazine co-polymer (TQN) due to photo-oxidative degradation. Both copolymers were found to be considerably more stable than polythiophenes. Moreover, the effect of incorporation of a thiophene-hexylthiophene moiety into the TQ1 or TQN backbone was studied, which resulted in a more black polymer with good absorption at all visible wavelengths. The TQN-thiophene-hexylthiophene copolymers displayed good stability against photo-oxidative degradation as well as an improved photovoltaic performance as compared to neat TQN. Finally, the rate of degradation of the investigated co-polymers was found to be independent of molecular weight or film thickness.

Control of the nanostructure is crucial for the performance of polymer:fullerene solar cells. The nanostructure achieved after film deposition from solution is not at equilibrium and tends to change upon annealing. Therefore, it is essential to improve the thermal stability of the active layer blend in order to facilitate high-speed printing processes. Two temperature regimes have to be considered. It was shown that mild heat treatment below the glass transition temperature of the blend resulted in local conformational changes of TQ1, which raised the power

## Concluding remarks

conversion efficiency of corresponding TQ1:PC<sub>61</sub>BM solar cells. In contrast, annealing above the glass transition temperature of the blend caused a detrimental decrease in device performance due to rapid coarsening of the blend nanostructure as well as the growth of micrometre-sized fullerene crystals. Careful examination of the PC<sub>61</sub>BM crystallisation kinetics in TQ1:PC<sub>61</sub>BM thin films revealed that the formation of large fullerene crystals was the result of insufficient nucleation. In this thesis, two routes were proposed that permit to improve the thermal stability of the blend nanostructure. Firstly, the PC<sub>61</sub>BM nucleation rate can be significantly increased through addition of unsubstituted C<sub>60</sub>-fullerene, which acts as a nucleating agent. Secondly, the use of fullerene mixtures effectively hinders crystallisation. Both approaches permit to strongly improve the photovoltaic performance of heat-treated TQ1:PC<sub>61</sub>BM active layers.

It is anticipated that the findings presented in this thesis are applicable to a wide range of other polymer:fullerene systems and, hence, will prove valuable for the further development of PSCs. During the last 10 years, the efficiency of PSCs has strongly increased, which together with improved thermal stability of the blend nanostructure may facilitate the large-scale production of PSCs.

## ACKNOWLEDGEMENTS

---

First of all I would like to thank Mats Andersson for accepting me as a PhD student almost 4.5 years ago and for the guidance and support during my years here at Chalmers.

For all encouragement and help, I would like to thank Christian Müller. Without your guidance, this thesis would probably not be what it is today. I have really enjoyed being a part of your group and all our discussions throughout the projects.

During my years as a PhD student, I have met many people that in one way or the other have contributed to this work. Especially, I would like to thank all co-authors of the papers included in this thesis. I would like to acknowledge Jonas Bergqvist (from the group of Olle Inganäs, Linköping) and Olof Bäcke (from the group of Eva Olsson, Chalmers), I have really liked working with you and your help has been invaluable! In addition, I would like to thank Patrik Henriksson for helping out with the photo-oxidative study.

Frida Andersson, Carina Pettersson, Christina Meyer, Anne Wendel, Ann Jacobsson, Kicki Stensvik, Anders Mårtensson and Roger Forsman, thanks for making the life at Applied Chemistry much easier!

To all former and present colleges at floor 8, I would like to send a big “thank you” for making my time here so enjoyable. Especially I would like to thank Zandra George, Markus Jarvid and Mattias Andersson for being such good friends. All things we have done during the years have really made my years as a PhD student special. To the people having coffee and lunch with me (you know who you are!); thanks for all the laughter and crazy discussions. Wenliu Zheng, you have been the best roommate ever, I really liked sharing the office with you. Renee Kroon, Tim Steckler, Ergang Wang and Sandra Fusco, all the help you have provided during the years have meant a lot for me, especially at the beginning of my PhD. Renee, I really enjoy discussing science with you so I hope we can

## Acknowledgements

continue with that also after this thesis is finished. Amaia Diaz de Zerio Mendaza, I have really enjoyed getting to know you, I'm very thankful for your support and friendship.

I am so grateful for my friends and family outside the world of Chalmers, without you this thesis would not exist. I want to thank my parents for always believing in me and supporting me no matter what.

At last, Christoffer, thanks for always being there, for the support you give me and for always making me laugh even through hard times. I love you!

## REFERENCES

---

1. <http://www.eia.gov/forecasts/aeo/er/?src=Total-f3>,  
*accessed* 20/05/13.
2. [http://ec.europa.eu/clima/policies/brief/causes/index\\_en.htm](http://ec.europa.eu/clima/policies/brief/causes/index_en.htm), *accessed*  
23/12/13.
3. S. Sartori, *MRS Bulletin*, 2013, **38**, 1011.
4. Nordic Energy Technology Perspective - Pathways to a Carbon Neutral  
Energy Future; International Energy Agency and Norden (Nordic Energy  
Research), 2013.
5. Z. He, C. Zhong, S. Su, M. Xu, H. Wu and Y. Cao, *Nature Photonics*,  
2012, **6**, 591-595.
6. S. H. Liao, H. J. Jhuo, Y. S. Cheng and S. A. Chen, *Adv. Mater.*, 2013,  
**25**, 4766-4771.
7. G. Yu and A. J. Heeger, *J. Appl. Phys.*, 1995, **78**, 4510-4515.
8. J. J. M. Halls, C. A. Walsh, N. C. Greenham, E. A. Marsegila, R. H.  
Friend, S. C. Moratti and A. B. Holmes, *Nature*, 1995, **376**, 498-500.
9. W. J. E. Beek, M. M. Wienk and R. A. J. Janssen, *J. Mater. Chem.*, 2005,  
**15**, 2985.
10. H. Kallmann and M. Pope, *J. Chem. Phys.*, 1959, **30**, 585.
11. J. A. Love, C. M. Proctor, J. Liu, C. J. Takacs, A. Sharenko, T. S. van der  
Poll, A. J. Heeger, G. C. Bazan and T.-Q. Nguyen, *Adv. Funct. Mater.*,  
2013, **23**, 5019-5026.
12. J. Yang, F. Guo, J. Hua, X. Li, W. Wu, Y. Qu and H. Tian, *J. Mater.*  
*Chem.*, 2012, **22**, 24356.
13. M. Hatano, S. Kambara and S. Okamoto, *J. Polym. Sci.*, 1961, **51**, S26-  
S29.
14. Jewett and Serway, *Physics For Scientists and Engineers with Mordern*  
*Physics*, Harris, David, 2004.
15. H. Shirakawa, E. J. Louis, A. G. MacDiarmid, C. K. Chiang and A. J.  
Heeger, *J.C.S. Chem. Comm.*, 1977, 578-580.
16. H. Shirakawa, *Nobel Lecture*, 2000.
17. C. J. Brabec, S. Gowrisanker, J. J. Halls, D. Laird, S. Jia and S. P.  
Williams, *Adv. Mater.*, 2010, **22**, 3839-3856.
18. E. E. Havinga, W. Hovee and H. Wynberg, *Polymer Bulletin*, 1992, **29**,  
119-126.
19. R. Kroon, *Synthesis and properties of  $\pi$ -conjugated polymers for organic*  
*photovoltaics*, Department of Chemical and Biological Engineering,  
Chalmers University of Technology, 2013.
20. P. Schilinsky, U. Asawapirom, U. Scherf, M. Biele and C. J. Brabec,  
*Chem. Mater.*, 2005, **17**, 2175-2180.
21. C. Müller, E. Wang, L. M. Andersson, K. Tvingstedt, Y. Zhou, M. R.  
Andersson and O. Inganäs, *Adv. Funct. Mater.*, 2010, **20**, 2124-2131.

## References

22. Y. Zhou, D. Antenehe Gedefaw, S. Hellström, I. Krätschmer, F. Zhang, W. Mammo, O. Inganäs and M. R. Andersson, *IEEE Journal of Selected Topics in Quantum Electronics*, 2010, **16**, 1565-1572.
23. E. Wang, L. Hou, Z. Wang, S. Hellström, F. Zhang, O. Inganäs and M. R. Andersson, *Adv. Mater.*, 2010, **22**, 5240-5244.
24. Y. Kim, H. R. Yeom, J. Y. Kim and C. Yang, *Energy & Environmental Science*, 2013, **6**, 1909.
25. J. C. Hummelen, B. W. Knight, F. LePeq, F. Wudl, J. Yao and C. L. Wilkins, *J. Org. Chem.*, 1995, **60**, 532-538.
26. M. M. Wienk, J. M. Kroon, W. J. Verhees, J. Knol, J. C. Hummelen, P. A. van Hal and R. A. Janssen, *Angew. Chem. Int. Ed.*, 2003, **42**, 3371-3375.
27. M. Lenes, G.-J. A. H. Wetzelaer, F. B. Kooistra, S. C. Veenstra, J. C. Hummelen and P. W. M. Blom, *Adv. Mater.*, 2008, **20**, 2116-2119.
28. M. Lenes, S. W. Shelton, A. B. Sieval, D. F. Kronholm, J. C. Hummelen and P. W. M. Blom, *Adv. Funct. Mater.*, 2009, **19**, 3002-3007.
29. Y. He, H.-Y. Chen, J. Hou and Y. Li, *J. Am. Chem. Soc.*, 2010, **132**, 1377-1382.
30. Z. Ma, E. Wang, K. Vandewal, M. R. Andersson and F. Zhang, *Appl. Phys. Lett.*, 2011, **99**, 143302.
31. S. Bertho, I. Haeldermans, A. Swinnen, W. Moons, T. Martens, L. Lutsen, D. Vanderzande, J. Manca, A. Senes and A. Bonfiglio, *Sol. Energy Mater. Sol. Cells*, 2007, **91**, 385-389.
32. B. Conings, S. Bertho, K. Vandewal, A. Senes, J. D'Haen, J. Manca and R. A. J. Janssen, *Appl. Phys. Lett.*, 2010, **96**, 163301.
33. J. Bergqvist, C. Lindqvist, O. Bäcké, Z. Ma, Z. Tang, W. Tress, S. Gustafsson, E. Wang, E. Olsson, M. R. Andersson, O. Inganäs and C. Müller, *J. Mater. Chem. A*, 2014.
34. B. R. Weinberger, M. Akhtar and S. C. Gau, *Synth. Met.*, 1982, **4**, 187-197.
35. C. W. Tang, *Appl. Phys. Lett.*, 1986, **48**, 183.
36. N. S. Sariciftci, D. Braun, C. Zhang, V. I. Srdanov, A. J. Heeger, G. Stucky and F. Wudl, *Appl. Phys. Lett.*, 1993, **62**, 585-587.
37. G. Yu, J. Gao, J. C. Hummelen, F. Wudl and A. J. Heeger, *Science*, 1995, **270**, 1789-1791.
38. X. Yang, J. K. J. van Duren, R. A. J. Janssen, M. A. J. Michels and J. Loos, *Macromolecules*, 2004, **37**, 2151-2158.
39. C. He, D. S. Germack, R. Joseph Kline, D. M. Delongchamp, D. A. Fischer, C. R. Snyder, M. F. Toney, J. G. Kushmerick and L. J. Richter, *Sol. Energy Mater. Sol. Cells*, 2011, **95**, 1375-1381.
40. C. Müller, J. Bergqvist, K. Vandewal, K. Tvingstedt, A. S. Anselmo, R. Magnusson, M. I. Alonso, E. Moons, H. Arwin, M. Campoy-Quiles and O. Inganäs, *J. Mater. Chem.*, 2011, **21**, 10676-10684.
41. C. Lindqvist, A. Sanz-Velasco, E. Wang, O. Bäcké, S. Gustafsson, E. Olsson, M. R. Andersson and C. Müller, *J. Mater. Chem. A*, 2013, **1**, 7174.



## References

42. M. Berggren, G. Gustafsson, O. Inganäs, M. R. Andersson, O. Wennerström and T. Hjertberg, *Appl. Phys. Lett.*, 1994, **65**, 1489.
43. S. Miller, G. Fanchinu, Y.-Y. Lin, C. Li, C.-W. Chen, W.-F. Su and M. Chhowalla, *J. Mater. Chem.*, 2008, **18**, 306-312.
44. F. Padinger, R. S. Rittberger and N. S. Sariciftci, *Adv. Funct. Mater.*, 2003, **13**, 85-88.
45. M. Campoy-Quiles, T. Ferenczi, T. Agostinelli, P. G. Etchegoin, Y. Kim, T. D. Anthopoulos, P. N. Stavrinou, D. D. C. Bradley and J. Nelson, *Nature Materials*, 2008, **7**, 158-164.
46. J. M. G. Cowie and V. Arrighi, *Polymers: Chemistry and Physics of Modern Materials*, CRC Press, 2008.
47. U. W. Gedde, *Polymer Physics*, Kluwer Academic Publishers, 1995.
48. F. C. Krebs, *Sol. Energy Mater. Sol. Cells*, 2009, **93**, 465-475.
49. T. Kugler, W. R. Salaneck, H. Rost and A. B. Holmes, *Chem. Phys. Lett.*, 1999, **310**, 391-396.
50. V. Shrotriya, G. Li, Y. Yao, C.-W. Chu and Y. Yang, *Appl. Phys. Lett.*, 2006, **88**, 073508.
51. R. Kroon, R. Gehlhaar, T. T. Steckler, P. Henriksson, C. Müller, J. Bergqvist, A. Hadipour, P. Heremans and M. R. Andersson, *Sol. Energy Mater. Sol. Cells*, 2012, **105**, 280-286.
52. C. J. Brabec, S. E. Shaheen, C. Winder, N. S. Sariciftci and P. Denk, *Appl. Phys. Lett.*, 2002, **80**, 1288.
53. Z. Tang, L. M. Andersson, Z. George, K. Vandewal, K. Tvingstedt, P. Heriksson, R. Kroon, M. R. Andersson and O. Inganäs, *Adv. Mater.*, 2012, **24**, 554-558.
54. J. J. M. Halls, K. Pichler, R. H. Friend, S. C. Moratti and A. B. Holmes, *Appl. Phys. Lett.*, 1996, **68**, 3120.
55. L. A. A. Pettersson, L. S. Roman and O. Inganäs, *J. Appl. Phys.*, 1999, **86**, 487.
56. M. Theander, A. Yartsev, D. Zigmantas, V. Sundström, W. Mammo, M. R. Andersson and O. Inganäs, *Phys. Rev. B*, 2000, **61**, 12957-12963.
57. D. Veldman, S. C. J. Meskers and R. A. J. Janssen, *Adv. Funct. Mater.*, 2009, **19**, 1939-1948.
58. K. Vandewal, K. Tvingstedt, A. Gadisa, O. Inganäs and J. V. Manca, *Nature Materials*, 2009, **8**, 904-909.
59. K. Norrman and F. C. Krebs, *Sol. Energy Mater. Sol. Cells*, 2006, **90**, 213-227.
60. F. C. Krebs, *Org. Electron.*, 2009, **10**, 761-768.
61. K. Kawano, R. Pacios, D. Poplavskyy, J. Nelson, D. D. C. Bradley and J. R. Durrant, *Sol. Energy Mater. Sol. Cells*, 2006, **90**, 3520-3530.
62. M. Jørgensen, K. Norrman, S. A. Gevorgyan, T. Tromholt, B. Andreasen and F. C. Krebs, *Adv. Mater.*, 2012, **24**, 580-612.
63. S. R. Dupont, M. Oliver, F. C. Krebs and R. H. Dauskardt, *Sol. Energy Mater. Sol. Cells*, 2012, **97**, 171-175.
64. D. M. Tanenbaum, H. F. Dam, R. Rösch, M. Jørgensen, H. Hoppe and F. C. Krebs, *Sol. Energy Mater. Sol. Cells*, 2012, **97**, 157-163.

## References

65. F. C. Krebs, *Sol. Energy Mater. Sol. Cells*, 2009, **93**, 2009.
66. R. Søndergaard, M. Hösel, D. Angmo, T. T. Larsen-Olsen and F. C. Krebs, *Materials Today*, 2012, **15**, 36-49.
67. C. E. Small, S. Chen, J. Subbiah, C. M. Amb, S.-W. Tsang, T.-H. Lai, J. R. Reynolds and F. So, *Nature Photonics*, 2012, **6**, 115-120.
68. H. Neugebauer, C. J. Brabec, J. C. Hummelen, R. A. J. Janssen and N. S. Sariciftci, *Synth. Met.*, 1999, **102**, 1002-1003.
69. M. O. Reese, A. M. Nardes, B. L. Rupert, R. E. Larsen, D. C. Olson, M. T. Lloyd, S. E. Shaheen, D. S. Ginley, G. Rumbles and N. Kopidakis, *Adv. Funct. Mater.*, 2010, **20**, 3476-3483.
70. A. Rivaton, S. Chambon, M. Manceau, J.-L. Gardette, N. Lemaître and S. Guillerez, *Polym. Degrad. Stabil.*, 2010, **95**, 278-284.
71. D. M. de Leeuw, M. M. J. Simenon, A. R. Brown and R. E. F. Einerhand, *Synth. Met.*, 1997, **87**, 53-59.
72. T. D. Anthopoulos, G. C. Anyfantis, G. C. Papavassiliou and D. M. de Leeuw, *Appl. Phys. Lett.*, 2007, **90**, 122105.
73. J. E. Carlé, M. Jørgensen, M. Manceau, M. Helgesen, O. Hagemann, R. Søndergaard and F. C. Krebs, *Sol. Energy Mater. Sol. Cells*, 2011, **95**, 3222-3226.
74. B. S. Ong, Y. Wu, P. Liu and S. Gardner, *J. Am. Chem. Soc.*, 2004, **126**, 3378-3379.
75. M. Manceau, E. Bundgaard, J. E. Carlé, O. Hagemann, M. Helgesen, R. Søndergaard, M. Jørgensen and F. C. Krebs, *J. Mater. Chem.*, 2011, **21**, 4132.
76. M. Manceau, A. Rivaton, J.-L. Gardette, S. Guillerez and N. Lemaître, *Polym. Degrad. and Stabil.*, 2009, **94**, 898-907.
77. S. Chambon, A. Rivaton, J. L. Gardette, M. Firon and L. Lutsen, *J. Polym. Sci. A Polym. Chem.*, 2007, **45**, 317-331.
78. H. Hintz, H. J. Egelhaaf, H. Peisert and T. Chassé, *Polym. Degrad. Stabil.*, 2010, **95**, 818-825.
79. D. J. D. Moet, M. Lenes, J. D. Kotlarski, S. C. Veenstra, J. Sweelssen, M. M. Koetse, B. de Boer and P. W. M. Blom, *Org. Elect.*, 2009, **10**, 1275-1281.
80. S. Chambon, A. Rivaton, J. L. Gardette and M. Firon, *Sol. Energy Mater. Sol. Cells*, 2007, **91**, 394-398.
81. A. S. Anselmo, *Materials aspects in spin-coated films for polymer photovoltaics*, Department of Engineering and Physics, Karlstad University, 2013.
82. M. Manceau, M. Helgesen and F. C. Krebs, *Polym. Degrad. Stabil.* , 2010, **95**, 266-2669.
83. J. Murphy, *Additives for Plastic Handbook*, Elsevier Science Ltd, 2001.
84. A. B. Strong, *Plastics: materials and processing*, Pearson Education, 2006.
85. T. Mustonen and N. Chebotareva, *WO 2012/095796 A1*, 2012.
86. G. Li, V. Shrotriya, J. Huang, Y. Yao, T. Moriarty, K. Emery and Y. Yang, *Nature Materials*, 2005, **4**, 864.

## References

87. M. O. Reese, S. A. Gevorgyan, M. Jørgensen, E. Bundgaard, S. R. Kurtz, D. S. Ginley, D. C. Olson, M. T. Lloyd, P. Morvillo, E. A. Katz, A. Elschner, O. Haillant, T. R. Currier, V. Shrotriya, M. Hermenau, M. Riede, K. R. Kirov, G. Trimmel, T. Rath, O. Inganäs, F. Zhang, M. Andersson, K. Tvingstedt, M. Lira-Cantu, D. Laird, C. McGuinness, S. Gowrisanker, M. Pannone, M. Xiao, J. Hauch, R. Steim, D. M. DeLongchamp, R. Rösch, H. Hoppe, N. Espinosa, A. Urbina, G. Yaman-Uzunoglu, J.-B. Bonekamp, A. J. J. M. van Breemen, C. Girotto, E. Voroshazi and F. C. Krebs, *Sol. Energy Mater. Sol. Cells*, 2011, **95**, 1253-1267.
88. B. Azzopardi, C. J. M. Emmott, A. Urbina, F. C. Krebs, J. Mutale and J. Nelson, *Energy & Environmental Science*, 2011, **4**, 3741.
89. B. Fillon, A. Thierry, B. Lotz and J. C. Wittmann, *J. Thermal Anal.*, 1994, **42**, 721-731.
90. W. Ma, C. Yang, X. Gong, K. Lee and A. J. Heeger, *Adv. Funct. Mater.*, 2005, **15**, 1617-1622.
91. T. J. Savenije, J. E. Kroeze, X. Yang and J. Loos, *Adv. Funct. Mater.*, 2005, **15**, 1260-1266.
92. C. Müller, T. A. M. Ferenczi, M. Campoy-Quiles, J. M. Frost, D. D. C. Bradley, P. Smith, N. Stingelin-Stutzmann and J. Nelson, *Adv. Mater.*, 2008, **20**, 3510-3515.
93. R. Dabirian, X. Feng, L. Ortolani, A. Lisco, V. Morandi, K. Müllen, P. Samorí and V. Palermo, *Phys. Chem. Chem. Phys.*, 2010, **12**, 4473-4480.
94. L. Zheng and Y. Han, *J. Phy. Chem. B*, 2012, **116**, 1598-1604.
95. A. Swinnen, I. Haeldermans, M. vande Ven, J. D'Haen, G. Vanhoyland, S. Aresu, M. D'Olieslaeger and J. Manca, *Adv. Funct. Mater.*, 2006, **16**, 760-765.
96. S. Bertho, G. Janssen, T. J. Cleij, B. Conings, W. Moons, A. Gadisa, J. D'Haen, E. Goovaerts, L. Lutsen, J. Manca and D. Vanderzande, *Sol. Energy Mater. Sol. Cells*, 2008, **92**, 753-760.
97. B. J. Kim, Y. Miyamoto, B. W. Ma and J. M. J. Frechet, *Adv. Funct. Mater.*, 2009, **19**, 2273-2281.
98. J. E. Carlé, B. Andreasen, T. Tromholt, M. V. Madsen, K. Norrman, M. Jørgensen and F. C. Krebs, *J. Mater. Chem.*, 2012, **22**, 24417.
99. S. Bertho, B. Campo, F. Piersimoni, D. Spoltore, J. D'Haen, L. Lutsen, W. Maes, D. Vanderzande and J. Manca, *Sol. Energy Mater. Sol. Cells*, 2013, **110**, 69-76.
100. Z. Li, H. C. Wong, Z. Huang, H. Zhong, C. H. Tan, W. C. Tsoi, J. S. Kim, J. R. Durrant and J. T. Cabral, *Nature Communications*, 2013, **4**, 2227.
101. F. Piersimoni, G. Degutis, S. Bertho, K. Vandewal, D. Spoltore, T. Vangerven, J. Drijkoningen, M. K. Van Bael, A. Hardy, J. D'Haen, W. Maes, D. Vanderzande, M. Nesladek and J. Manca, *J. Polym. Sci. B Polym. Phys.*, 2013, **51**, 1209-1214
102. X. Yang, A. Alexeev, M. A. J. Michels and J. Loos, *Macromolecules*, 2005, **38**, 4289-4295.

## References

103. J. Zhao, A. Swinnen, G. V. Assche, J. Manca, D. Vanderzande and B. V. Mele, *J. Phys. Chem. B*, 2009, **113**, 1587-1591.
104. T. T. Ngo, D. N. Nguyen and V. T. Nguyen, *Advances in Natural Sciences: Nanoscience and Nanotechnology*, 2012, **3**, 045001.
105. P. E. Hopkinson, P. A. Staniec, A. J. Pearson, A. D. F. Dunbar, T. Wang, A. J. Ryan, R. A. L. Jones, D. G. Lidzey and A. M. Donald, *Macromolecules*, 2011, **44**, 2908-2917.
106. E. Verploegen, R. Mondal, C. J. Bettinger, S. Sok, M. F. Toney and Z. Bao, *Adv. Funct. Mater.*, 2010, **20**, 3519-3529.
107. R. Kroon, R. Gehlhaar, T. T. Steckler, P. Henriksson, C. Müller, J. Bergqvist, A. Hadipour, P. Heremans and M. R. Andersson, *Sol. Energy Mater. Sol. Cells*, 2012, **105**, 280-286.
108. E. Wang, J. Bergqvist, K. Vandewal, Z. Ma, L. Hou, A. Lundin, S. Himmelberger, A. Salleo, C. Müller, O. Inganäs, F. Zhang and M. R. Andersson, *Adv. Energy Mater.*, 2013, **3**, 806-814.
109. L. Hou, E. Wang, J. Bergqvist, B. V. Andersson, Z. Wang, C. Müller, M. Campoy-Quiles, M. R. Andersson, F. Zhang and O. Inganäs, *Adv. Funct. Mater.*, 2011, **21**, 3169-3175.
110. G. Hägg, *Allmän och oorganisk kemi*, Almqvist & Wiksells, 1963.
111. J. A. Kalb, in *Phase Change Materials*, eds. S. Raoux and M. Wuttig, 2009, pp. 125-148.
112. M. W. M. Kristiansen, T. Tervoort, P. Smith, M. Blomenhofer, H. W. Schmidt, *Macromolecules*, 2003, **36**, 5150-5156.
113. S. G. M. Blomenhofer, D. Hanft, H. W. Schmidt, M. Kristiansen, P. Smith, K. Stoll, D. Mader, K. Hoffmann, *Macromolecules*, 2005, **38**, 3688-3695.
114. K. Bernland, T. Tervoort and P. Smith, *Polymer*, 2009, **50**, 2460-2464.
115. N. D. Treat, J. A. N. Malik, O. Reid, L. Yu, C. G. Shuttle, G. Rumbles, C. J. Hawker, M. L. Chabinyc, P. Smith and N. Stingelin, *Nature Materials*, 2013.
116. J. J. Richards, A. H. Rice, R. D. Nelson, F. S. Kim, S. A. Jenekhe, C. K. Luscombe and D. C. Pozzo, *Adv. Funct. Mater.*, 2013, **23**, 514-522.
117. M. A. Faist, P. E. Keivanidis, S. Foster, P. H. Wöbkenberg, T. D. Anthopoulos, D. D. C. Bradley, J. R. Durrant and J. Nelson, *J. Polym. Sci. B Polym. Phys.*, 2011, **49**, 45-51.
118. H. W. Liu, D. Y. Chang, W. Y. Chiu, S. P. Rwei and L. Wang, *J. Mater. Chem.*, 2012, **22**, 15586-15591.
119. C. Y. Chen, C. S. Tsao, Y. C. Huang, H. W. Liu, W. Y. Chiu, C. M. Chuang, U. S. Jeng, C. J. Su, W. R. Wu, W. F. Su and L. Wang, *Nanoscale*, 2013, **5**, 7629-7638.
120. Y. Santo, I. Jeon, K. S. Yeo, T. Nakagawa and Y. Matsuo, *Appl. Phys. Lett.*, 2013, **103**, 073306.